Article

Specification of CNS macrophage subsets occurs postnatally in defined niches

https://doi.org/10.1038/s41586-022-04596-2

Received: 30 November 2020

Accepted: 28 February 2022

Published online: 20 April 2022

Check for updates

Takahiro Masuda[1,2,22]✉, Lukas Amann[1,22], Gianni Monaco[1], Roman Sankowski[1,3], Ori Staszewski[1,3], Martin Krueger[4], Francesca Del Gaudio[5], Liqun He[6], Neil Paterson[7,8,9], Elisa Nent[7], Francisco Fernández-Klett[10], Ayato Yamasaki[2], Maximilian Frosch[1], Maximilian Fliegauf[1,11], Lance Fredrick Pahutan Bosch[1,9], Hatice Ulupinar[1,9], Nora Hagemeyer[1], Dietmar Schreiner[12], Cayce Dorrier[13,14], Makoto Tsuda[2], Claudia Grothe[12], Anne Joutel[15], Richard Daneman[13,14], Christer Betsholtz[6,16], Urban Lendahl[5], Klaus-Peter Knobeloch[1,17], Tim Lämmermann[7], Josef Priller[10,18,19,23], Katrin Kierdorf[1,17,20,23] & Marco Prinz[1,20,21,23]✉

All tissue-resident macrophages of the central nervous system (CNS)—including parenchymal microglia, as well as CNS-associated macrophages (CAMs[1]) such as meningeal and perivascular macrophages[2–7]—are part of the CNS endogenous innate immune system that acts as the first line of defence during infections or trauma[2,8–10]. It has been suggested that microglia and all subsets of CAMs are derived from prenatal cellular sources in the yolk sac that were defined as early erythromyeloid progenitors[11–15]. However, the precise ontogenetic relationships, the underlying transcriptional programs and the molecular signals that drive the development of distinct CAM subsets in situ are poorly understood. Here we show, using fate-mapping systems, single-cell profiling and cell-specific mutants, that only meningeal macrophages and microglia share a common prenatal progenitor. By contrast, perivascular macrophages originate from perinatal meningeal macrophages only after birth in an integrin-dependent manner. The establishment of perivascular macrophages critically requires the presence of arterial vascular smooth muscle cells. Together, our data reveal a precisely timed process in distinct anatomical niches for the establishment of macrophage subsets in the CNS.

Both perivascular macrophages and meningeal macrophages have been shown to be derived from prenatal erythromyeloid progenitors (EMPs) in the yolk sac and are long-lived with self-renewing capacity[11], as is the case for microglia[12,13]. Around the age of 8.5 days after conception (embryonic day (E) 8.5) in mice, EMPs appear in the extra-embryonic yolk sac blood islands. They differentiate thereafter into A2 pre-macrophage progenitors via immature A1 progenitors[13,14,16]. From E9.5 on, these progenitors start to migrate and colonize the developing CNS[11,15]. During adulthood, microglia and CAMs can clearly be distinguished by their location and distinct core transcriptomic signatures. These include high gene expression of *Tmem119*, *Hexb*, *Siglech*, *Slc2a5*, *P2ry12*, *Fcrls*, *Sall1* and *Trem2* in microglia, whereas CAMs are characterized by high levels of mRNA expression of *Mrc1*, *Lyve1*, *Cd163*, *Siglec1* and *Ms4a7* (refs. [1,7,17–19]). However, the precise ontogenetic relationships between CAMs and microglia remain poorly understood. Here we comprehensively characterize the distribution, kinetics, gene expression profiles and fates of perivascular and meningeal macrophages as well as microglia during the course of development, and elucidate the cellular machineries that drive the establishment of distinct CNS macrophages at specific time points and in distinct anatomical niches.

Distinct developmental kinetics of CAMs

We first examined the distribution of CNS macrophages during development in *Cx3cr1*$^{GFP/+}$ mice. As reported previously[13,15], IBA1^{+}GFP^{+} microglia were observed in the brain parenchyma at all time points, albeit with changing morphologies and densities (Fig. 1a, b). In contrast to

[1]Institute of Neuropathology, Faculty of Medicine, University of Freiburg, Freiburg, Germany. [2]Department of Molecular and System Pharmacology, Graduate School of Pharmaceutical Sciences, Kyushu University, Fukuoka, Japan. [3]Berta-Ottenstein-Programme for Clinician Scientists, Faculty of Medicine, University of Freiburg, Freiburg, Germany. [4]Institute of Anatomy, University of Leipzig, Leipzig, Germany. [5]Department of Cell and Molecular Biology, Karolinska Institute, Stockholm, Sweden. [6]Department of Immunology, Genetics and Pathology, Rudbeck Laboratory, Uppsala University, Uppsala, Sweden. [7]Max Planck Institute of Immunobiology and Epigenetics, Freiburg, Germany. [8]International Max Planck Research School for Immunobiology, Epigenetics and Metabolism (IMPRS-IEM), Freiburg, Germany. [9]Faculty of Biology, University of Freiburg, Freiburg, Germany. [10]Neuropsychiatry and Laboratory of Molecular Psychiatry, Charité – Universitätsmedizin Berlin, and DZNE, Berlin, Germany. [11]Department of Pharmaceutical Biology and Biotechnology, Institute of Pharmaceutical Sciences, University of Freiburg, Freiburg, Germany. [12]Institute of Neuroanatomy and Cell Biology, Hannover Medical School, Hannover, Germany. [13]Department of Neurosciences, University of California San Diego, San Diego, CA, USA. [14]Department of Pharmacology, University of California San Diego, San Diego, CA, USA. [15]Institute of Psychiatry and Neurosciences of Paris (IPNP), Inserm, University of Paris, Paris, France. [16]Department of Medicine Huddinge (MedH), Karolinska Institute, Huddinge, Sweden. [17]CIBSS – Centre for Integrative Biological Signalling Studies, University of Freiburg, Freiburg, Germany. [18]Department of Psychiatry and Psychotherapy, School of Medicine, Technical University of Munich, Munich, Germany. [19]University of Edinburgh and UK DRI, Edinburgh, UK. [20]Center for Basics in NeuroModulation (NeuroModulBasics), Faculty of Medicine, University of Freiburg, Freiburg, Germany. [21]Signalling Research Centres BIOSS and CIBSS, University of Freiburg, Freiburg, Germany. [22]These authors contributed equally: Takahiro Masuda, Lukas Amann. [23]These authors jointly supervised this work: Josef Priller, Katrin Kierdorf, Marco Prinz.
✉e-mail: masuda@phar.kyushu-u.ac.jp; marco.prinz@uniklinik-freiburg.de

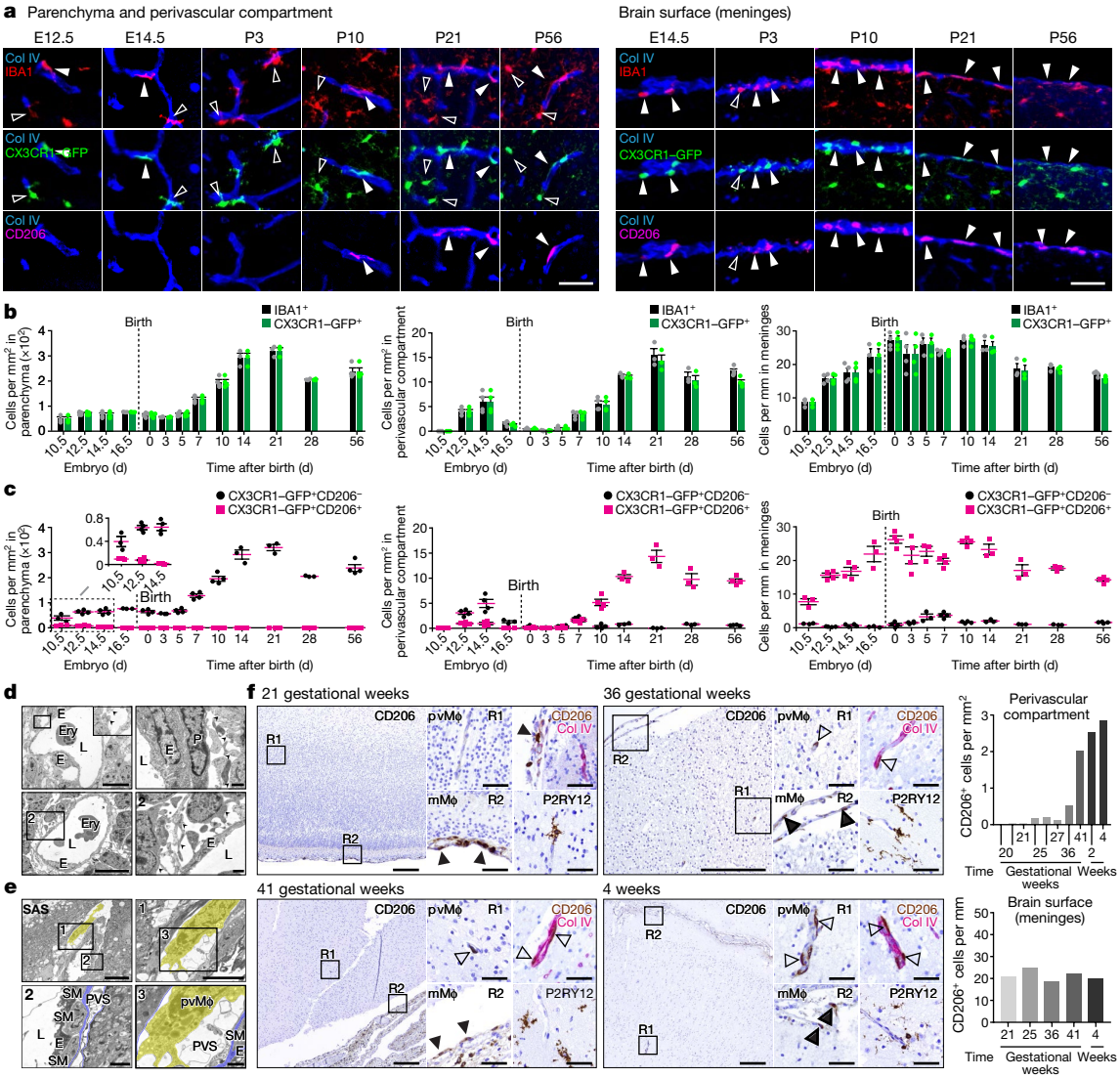

Fig. 1 | Perivascular and meningeal macrophages show distinct developmental patterns in mice and humans. a, Images showing the kinetics of IBA1$^+$ (red), CX3CR1–GFP$^+$ (green) and CD206$^+$ (purple) cells, combined with Col IV (blue), in each brain compartment (parenchyma, perivascular compartment and brain surface (meninges)) of the cortex of *Cx3cr1*$^{GFP/+}$ mice during development. Representative pictures out of three (P21) or four (E12.5, E14.5, P3, P10 and P56) mice investigated are shown. Scale bars, 50 µm. **b**, **c**, Quantification of IBA1$^+$ or CX3CR1–GFP$^+$ cells (**b**), and CX3CR1–GFP$^+$CD206$^+$ or CX3CR1–GFP$^+$CD206$^-$ cells (**c**), in each brain compartment of the *Cx3cr1*$^{GFP/+}$ brains during development ($n = 3$: E10.5, E16.5, P3, P14, P21 and P28; $n = 4$: E12.5, E14.5, P0, P5, P7, P10 and P56 for parenchyma and perivascular compartment; $n = 3$: E10.5, E16.5, P5, P14, P21 and P28; $n = 4$: E12.5, E14.5, P0, P3, P7, P10 and P56 for brain surface (meninges)) (mean ± s.e.m.). Symbols represent individual mice. **d**, **e**, Electron microscopy images depicting the composition of the vessel compartments in the brains of wild-type mice at E14.5 (**d**), or the establishment of basal laminas in the brains at P10 (**e**). Insets indicate high-magnification images. Filled and empty arrowheads indicate glial processes lacking basal lamina and vascular wall lacking basal lamina, respectively. Blue, outer vascular and glial basal lamina; yellow, perivascular macrophages. E, endothelial cell; Ery, erythrocyte; L, vascular lumen; P, pericyte; pvMΦ, perivascular macrophage; PVS, perivascular space; SAS, subarachnoid space; SM, smooth muscle cell. Representative pictures out of $n = 3$ (E14.5) or $n = 6$ (P10) mice investigated. Scale bars, 10 µm (**d**, left images; **e**, top left); 5 µm (**e**, bottom left); 2 µm (**e**, top right); 1 µm (**d**, right images; **e**, bottom right). **f**, Left and middle, representative immunohistochemistry of CD206$^+$ perivascular macrophages (pvMΦ; blank arrowheads), CD206$^+$ meningeal macrophages (mMΦ; filled arrowheads), Col IV$^+$ blood vessels (red) and P2RY12$^+$ microglia (brown) in the developing human cortex. Insets indicate high-magnification images of perivascular macrophages (R1) or meningeal macrophages (R2). Images are representative of one sample per time point. Scale bars, 200 µm (left images); 50 µm (right insets). Right, quantification of CD206$^+$ perivascular macrophages and CD206$^+$ meningeal macrophages in the human cerebral cortex at the indicated time points. Bars represent individual embryos and infants.

CAMs, microglia were virtually negative for the mannose receptor C-type1 (MRC1, also known as CD206). Only at early embryonic time points (E10.5 and E12.5) did a larger fraction of microglia express CD206 (Fig. 1c), which is in line with previous studies[20,21]. In addition, IBA1$^+$GFP$^+$ myeloid cells were found in the collagen (Col) IV$^+$ perivascular compartment; the number of these cells peaked at E14.5 and they disappeared at birth. However, vessel-associated IBA1$^+$GFP$^+$ cells were detectable again at postnatal day (P) 7 and gradually increased over time. Notably, the embryonic population was largely CD206$^-$, whereas the postnatal population was mainly CD206$^+$, suggesting that these might be distinct populations of macrophages. In contrast, IBA1$^+$GFP$^+$ meningeal macrophages were detectable in the leptomeninges at all investigated time points—even at E10.5, at which point Col IV$^+$ meninges are being established during embryogenesis[22,23].

The perivascular macrophages are defined by their distinct location in the perivascular Virchow–Robin space, where they are sandwiched

between two basal laminas: one from the endothelial cells or basement membranes of mural cells (vascular smooth muscle cells (VSMCs) or pericytes) and the other from the astrocytic endfeet[2,11]. We thus examined the precise spatiotemporal development of the perivascular compartment by transmission electron microscopy. No basal lamina or VSMC-containing arteries or arterioles were present at E14.5 (Fig. 1d). Distinct spaces surrounding VSMC-containing arteries and arterioles only became apparent at P3 (Extended Data Fig. 1a) and at P10 (Fig. 1e), suggesting a postnatal development of the perivascular spaces in the brain. Consistently, the first typical perivascular macrophages were detected around P10 (Fig. 1e). Notably, most of the GFP$^+$ cells in the perivascular compartment of the *Cx3cr1*$^{GFP/+}$ brain at E14.5 were negative for the CAM marker lymphatic vessel endothelial hyaluronan receptor-1 (LYVE1)[17] but expressed the purinergic receptor P2Y12, a prototypical microglia marker (Extended Data Fig. 1b–d). Conversely, postnatal GFP$^+$ cells in the Virchow–Robin space at P10 were CD206$^+$LYVE1$^+$P2RY12$^-$, which is a cell phenotype that is characteristic of perivascular macrophages[1,11,17,19].

To extend our findings to the human brain, we examined the developmental kinetics of both meningeal macrophages and perivascular macrophages in human fetal and postnatal brain sections (Fig. 1f). CD206$^+$ meningeal macrophages were present at constant numbers at all time points examined (gestational week 20 to 4 weeks after birth), whereas CD206$^+$ perivascular macrophages were barely detectable before gestational week 25 in the fetal brain and markedly increased around and after the time of birth.

Together, these results suggest that in both mice and humans, the embryonic perivascular myeloid compartment is composed of vessel-associated microglia, whereas the postnatal wave represents classical perivascular macrophages. This developmental switch is accompanied by the concomitant establishment of the Virchow–Robin space.

Localization of perivascular macrophages

The CNS is nourished by a complex vascular network that comprises arteries, arterioles, capillaries, veins and venules, all of which have distinct features[24,25]. CD206$^+$ perivascular macrophages were found to be embedded within the laminin$^+$ vascular basement membranes (Extended Data Fig. 1e, f) that are ensheathed by astrocytic endfeet[26]. Of note, perivascular macrophages showed a characteristic distribution pattern, with preferential localization around alpha smooth muscle actin (aSMA)-positive and transferrin receptor (TfR)-negative arteries and arterioles in a sex-independent manner (Extended Data Fig. 1g). Although there was a minor population of perivascular macrophages colonizing the aSMA$^-$TfR$^+$ veins and venules, no perivascular macrophages surrounded capillaries. Consistently, GFP$^+$CD206$^+$ perivascular macrophages in *Cx3cr1*$^{GFP/+}$ mice were mainly associated with aSMA$^+$ arteries and arterioles that were also positive for SOX17 (ref. [27]) (Extended Data Fig. 1h), whereas very few GFP$^+$CD206$^+$ perivascular macrophages were localized around endomucin-positive capillaries, veins or venules[28] (Extended Data Fig. 1i, j). Additional electron microscopy examinations led to the same conclusion (Extended Data Fig. 1k, l). Similarly, CD206$^+$ perivascular macrophages in the human CNS were mainly present around arteries and arterioles at different time points starting from late gestational time points (Extended Data Fig. 1m). Together, these results demonstrate a preferential localization of perivascular macrophages within the perivascular spaces of arteries and arterioles in the postnatal mouse and human cortex.

HSC independence of CAMs during adulthood

In all three CNS compartments, IBA1$^+$GFP$^+$ cells possessed proliferative capacity, albeit to varying degrees and in a developmental-stage-dependent manner (Extended Data Fig. 2a–c). Although vessel-associated IBA1$^+$GFP$^+$ cells disappeared perinatally (Fig. 1b), GFP$^+$ cells did not undergo apoptosis at late embryonic time points (Extended Data Fig. 2d). We next pulsed *Cx3cr1*$^{CreERT2/+}$*R26*$^{YFP/YFP}$ pregnant mice with 4-hydroxy tamoxifen (4OH-TAM) at E9.5 to label *Cx3cr1*-expressing yolk sac progenitors (Extended Data Fig. 2e), resulting in permanent YFP expression in both fetal and neonatal microglia and CAMs[11,16]. At E14.5, IBA1$^+$YFP$^+$ cells were detectable in all compartments (Extended Data Fig. 2f, g). In contrast to the stable presence of IBA1$^+$YFP$^+$ cells in the parenchyma and meninges, the perivascular compartment was devoid of IBA1$^+$YFP$^+$ cells at P0, whereas IBA1$^+$YFP$^+$ perivascular cells emerged again at P14.

To examine the contribution of haematopoietic stem cell (HSC)-derived cells to the pool of CAMs, we used *Cxcr4*$^{CreERT-IRES-eGFP}$ (*Cxcr4*^{CreERT2}) mice. Injection of tamoxifen (TAM) into *Cxcr4*$^{CreERT2/+}$*Rosa26*$^{tdTomato/+}$ (*R26*^{tdT}) adult mice allowed the fate mapping of tdT-labelled HSC-derived cells[29,30] (Extended Data Fig. 2h) such as blood Ly6C^{hi} monocytes (Extended Data Fig. 2i). Of note, CD206$^+$ perivascular macrophages and meningeal macrophages, as well as microglia, were lacking tdT (Extended Data Fig. 2j, k) suggesting that HSC-derived cells make virtually no contribution to the populations of perivascular and meningeal macrophages under homeostatic conditions. By contrast, the number of tdT$^+$ cells among choroid plexus macrophages—which constitute an ontogenically and transcriptionally mixed population of CAMs[1,11]—increased over time (Extended Data Fig. 2j, k), indicating a partial engraftment of HSC-derived cells. In sum, microglia, perivascular macrophages and meningeal macrophages reside in the healthy adult mouse CNS without any input from peripheral HSC-derived precursors.

Stepwise developmental program of CAMs

To assess their transcriptional signatures during ontogeny, we performed a bulk RNA sequencing (RNA-seq) analysis of perivascular macrophages, meningeal macrophages and microglia isolated from *Cx3cr1*$^{GFP/+}$ brains at distinct developmental time points (Extended Data Fig. 3). A heat map of the top 10 differentially regulated genes per cluster revealed distinct gene expression patterns across CNS macrophages during the course of development (Extended Data Fig. 3a). Notably, microglial core genes (for example, *P2ry12*, *Tmem119* and *Hexb*) gradually increased in expression and reached their highest expression levels during adulthood (Extended Data Fig. 3b), whereas CAM core signature genes (for example, *Pf4*, *Lyve1* and *Mrc1*) peaked in meningeal macrophages at early postnatal time points and decreased at later stages (Extended Data Fig. 3c). Perivascular macrophages and meningeal macrophages expressed similar CAM signature genes at the same time points, albeit at lower expression levels in perivascular macrophages (Extended Data Fig. 3c). We observed few differences in the expression of transcription factors between CAMs and microglia (Extended Data Fig. 3d). Together, these data suggest a stepwise developmental program of CNS macrophages, in which core genes are established in meningeal macrophages at early time points, but microglia accomplish their full transcriptional repertoire at postnatal stages.

Mrc1^{CreERT2} mice to study CAMs

A lack of cell-type-specific targeting tools has hampered the definition and dissection of the precise ontogeny of CAMs, as well as their specific functions in health and disease. To genetically target CAMs, we generated a mouse line in which a T2A-CreERT2 cassette was inserted into the *Mrc1* locus (hereinafter referred to as *Mrc1*^{CreERT2}) (Extended Data Fig. 4a). As expected from previous approaches using a T2A-CreERT2 cassette[18], the insertion led to a reduction in the expression of *Mrc1* in CAMs from *Mrc1*$^{CreERT2/CreERT2}$ mice, whereas overall gene expression in CAMs was barely altered, with only a few differentially regulated genes that reached statistical difference (Extended Data Fig. 4b–d). Consistently, CAMs in *Mrc1*$^{CreERT2/CreERT2}$ mice—but not in *Mrc1*^{CreERT2} mice—showed

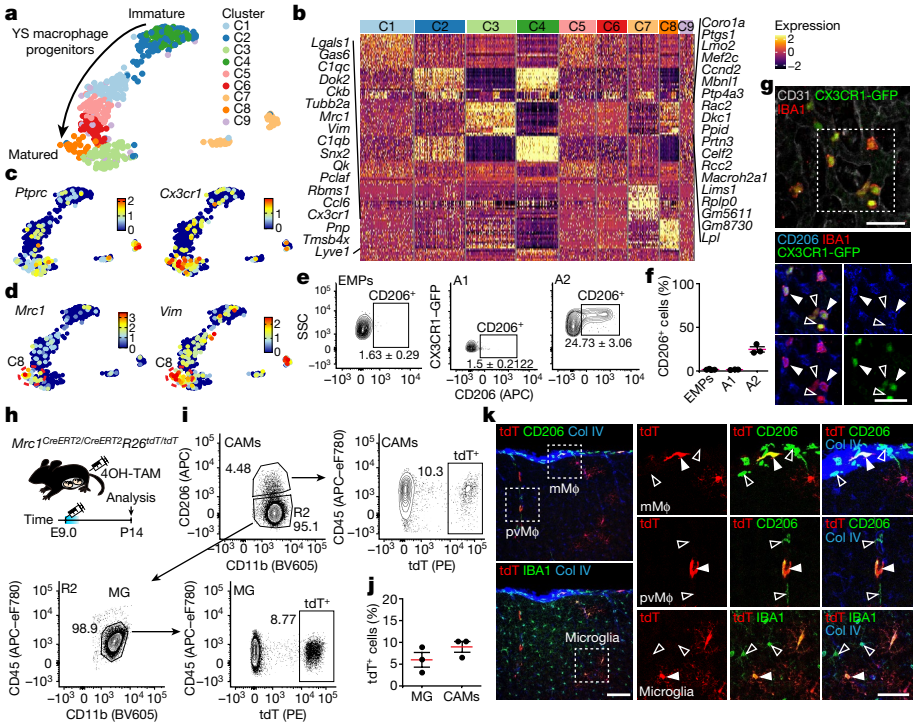

Fig. 2 | *Mrc1*-expressing A2 cells in the yolk sac are progenitors for both microglia and CAMs. a, Uniform manifold approximation and projection (UMAP) plot of 483 macrophage progenitors isolated from the yolk sac (YS) at E9.5 depicting nine individual clusters (C1–C9). Each dot represents an individual cell. Arrow indicates phenotypic shift of immature towards matured macrophage progenitors. **b**, Heat map of the 20 top differentially regulated genes in each cluster. **c**, UMAP plots depicting the distribution of *Ptprc* and *Cx3cr1* transcripts in yolk sac progenitors. **d**, UMAP plots depicting high expression levels of *Mrc1* and *Vim* transcripts in C8. **e**, Flow-cytometry-based measurement of CD206$^+$ cells among c-Kit$^+$AA4.1$^+$CD45$^{neg\text{-}lo}$F4/80$^-$ EMPs, c-Kit$^+$AA4.1$^-$CD45$^+$CX3CR1–GFP$^-$ A1 cells or c-Kit$^-$AA4.1$^-$CD45$^+$CX3CR1–GFP$^+$ A2 cells in yolk sacs from *Cx3cr1*$^{GFP/+}$ mice. Representative plots out of three (A1 or A2 at E9.5) or four (EMPs at E8.5) yolk sacs investigated. **f**, Quantification of **e** (mean ± s.e.m.). Symbols represent individual yolk sacs (EMPs, $n = 4$; A1/A2, $n = 3$). **g**, Images depicting CD206$^+$ A2 cells in the yolk sac of *Cxc3cr1*$^{GFP/+}$ pregnant females at E9.5. IBA1 (red), CD206 (blue) and CD31 for yolk sac endothelial cells (white) are shown. White filled and blank white arrowheads indicate CD206$^+$IBA1$^+$CX3CR1–GFP$^+$ or CD206$^-$IBA1$^+$CX3CR1–GFP$^+$ A2 cells, respectively. Scale bars, 50 µm (main image); 20 µm (inset). Representative pictures out of five yolk sacs investigated. **h**, Scheme of the experimental set-up. **i**, Flow-cytometry-based measurement of tdT$^+$ cells in CD45^{lo}CD11b$^+$CD206$^-$ microglia (MG) and CD11b$^+$CD206$^+$ CAMs in *Mrc1*$^{CreERT2/CreERT2}$*R26*$^{tdT/tdT}$ mice at P14. Representative plots out of three mice investigated. **j**, Quantification of **i** (mean ± s.e.m.). Symbols represent individual mice ($n = 3$). **k**, Immunofluorescence images showing tdT$^+$ microglia (IBA1$^+$), perivascular macrophages (CD206$^+$) or meningeal macrophages (CD206$^+$) in the *Mrc1*$^{CreERT2/CreERT2}$*R26*$^{tdT/tdT}$ mice at P14. Representative images out of four mice investigated. Scale bars, 100 µm (main image); 50 µm (inset).

a reduction in CD206 expression (Extended Data Fig. 4e, f), but cells from both genotypes did not show any further apparent alterations and exhibited a similar core gene expression pattern to wild-type CAMs (Extended Data Fig. 4g). Furthermore, CAMs and microglia from mutant mice were unchanged in number (Extended Data Fig. 4h), suggesting no obvious off-target effects. Detailed histological examination of *Mrc1*$^{CreERT2/+}$*R26*$^{tdT/tdT}$ and *Mrc1*$^{CreERT2/CreERT2}$*R26*$^{tdT/tdT}$ mice after administration of TAM revealed a high recombination efficiency in both perivascular macrophages and meningeal macrophages (Extended Data Fig. 4i–k). Of note, we did not observe any recombination in microglia, astrocytes, neurons or oligodendrocytes, or in circulating Ly6C^{hi} and Ly6C^{lo} monocytes, Ly6G$^+$ granulocytes, CD3e$^+$ T cells or CD19$^+$ B cells (Extended Data Fig. 4j–l). In summary, the *Mrc1*^{CreERT2} line provides a highly specific tool to target both perivascular macrophages and meningeal macrophages.

A common *Mrc1*$^+$ CAM and microglia progenitor

Both microglia and CAMs originate from early yolk sac progenitors[11]. However, it remains unknown as to whether they share a common progenitor, or whether distinct pre-committed precursors already exist in the yolk sac. To address this question, we performed single-cell RNA sequencing (scRNA-seq) to profile myeloid progenitor linages in the yolk sac (c-Kit^{lo}CD45$^+$) (refs. [13,16,31]) (Extended Data Fig. 5a). Unbiased clustering[32] of 483 analysed cells revealed the presence of 9 transcriptionally distinct clusters (Fig. 2a, b). The *Cx3cr1*^{lo}*Ptprc*^{lo} immature population constituted clusters C1, C2, C4, C5 and C6, whereas C3 and C8 were found in the *Cx3cr1*^{hi}*Ptprc*$^+$ matured yolk sac population (Fig. 2a, c). The C9 population was sparsely distributed, and C7 showed a monocyte or granulocyte signature (Extended Data Fig. 5b). The immature yolk sac population was transcriptionally further separated into two main clouds. One cloud (C2 and C4) was characterized by high expression of *Slc2a3* and *Apoa2*, whereas the other (C1, C5 and C6) highly expressed *Psat1* (Extended Data Fig. 5c). By contrast, the clusters C3 and C8 were transcriptionally distinct on the basis of the expression of genes including *Mrc1* and *Vim* (C3) or *Ccnd2* (C8) (Fig. 2d, Extended Data Fig. 5d). Flow cytometry analysis of yolk sac progenitors validated the presence of a CD206$^+$ subpopulation within the A2 population (Fig. 2e, f, Extended Data Fig. 5a, e), which was further visualized histologically (Fig. 2g, Extended Data Fig. 5f). These results raise the possibility that CD206$^+$ A2 macrophage progenitors could be the committed yolk sac progenitors for CAMs, as suggested previously[33]. To test this, we performed a fate-mapping analysis of the CD206$^+$ yolk sac subpopulation by injection of 4OH-TAM into *Mrc1*$^{CreERT2/CreERT2}$*R26*$^{tdT/tdT}$ mice at E9.0 (Fig. 2h). Notably, analysis of the offspring at P14 revealed the presence of tdT-positive cells in both microglia and CAMs (Fig. 2i–k). Comprehensive examinations of the yolk sac and fetal liver of *Mrc1*$^{CreERT2/CreERT2}$*R26*$^{tdT/tdT}$ mice did not reveal any transient recombination

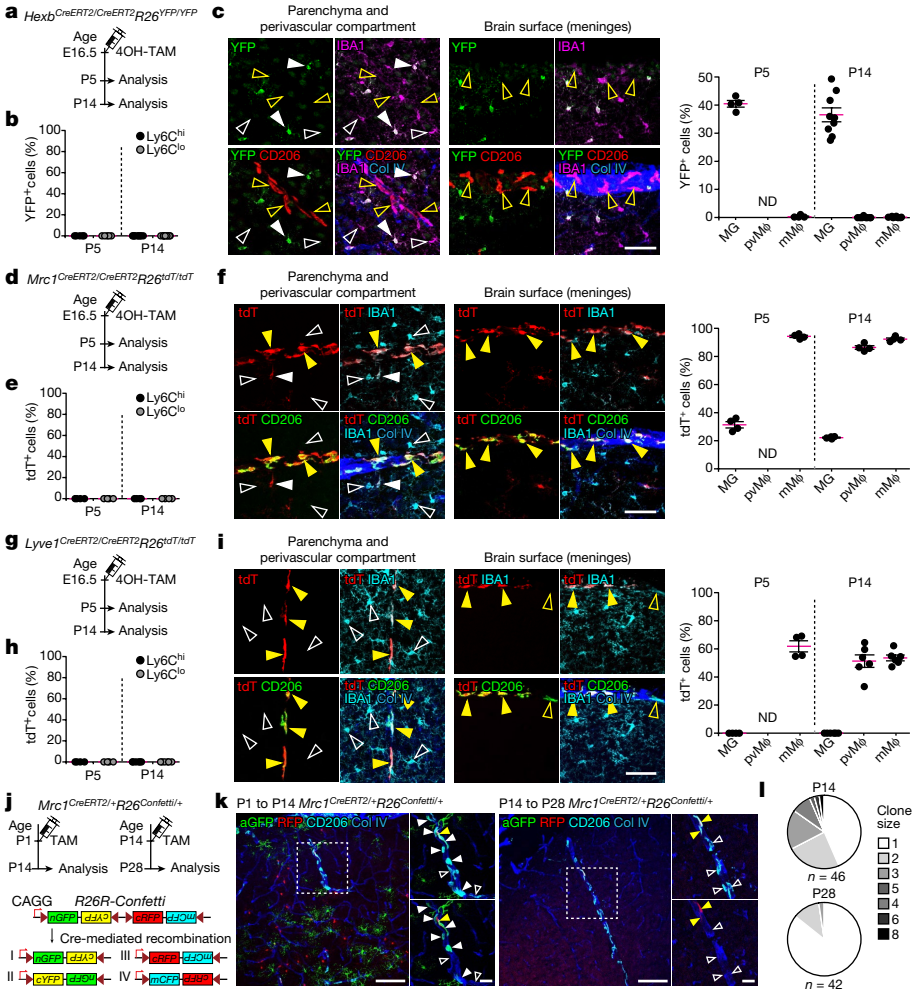

Fig. 3 | Meningeal macrophages are the source for perivascular macrophages in the postnatal perivascular niche. a, **d**, **g**, Scheme of the experimental set-up. **b**, **e**, **h**, Flow-cytometry-based quantification of labelled Ly6C^{hi} or Ly6c^{lo} blood monocytes in *Hexb*$^{CreERT2/CreERT2}$*R26*$^{YFP/YFP}$ mice (**b**; P5, $n = 5$; P14, $n = 9$), in *Mrc1*$^{CreERT2/CreERT2}$*R26*$^{tdT/tdT}$ mice (**e**; P5 and P14, $n = 4$) or in *Lyve1*$^{CreERT2/CreERT2}$*R26*$^{tdT/tdT}$ mice (**h**; P5, $n = 4$; P14, $n = 6$). Symbols represent individual mice (mean ± s.e.m.). **c**, **f**, **i**, Left, immunofluorescence images of YFP (green), IBA1 (purple) and CD206 (red) with Col IV (blue) from *Hexb*$^{CreERT2/CreERT2}$*R26*$^{YFP/YFP}$ mice (**c**), or tdT (red), IBA1 (light blue) and CD206 (green) with Col IV (blue) from *Mrc1*$^{CreERT2/CreERT2}$*R26*$^{tdT/tdT}$ mice (**f**) and *Lyve1*$^{CreERT2/CreERT2}$*R26*$^{tdT/tdT}$ mice (**i**) at P14. Arrowheads indicate double-positive (filled white) or single-positive (blank white) microglia and double-positive (filled yellow) or single-positive (blank yellow) perivascular macrophages or meningeal macrophages. Typical images from four (**c**, **f**) or six (**i**) mice are depicted. Right, quantification (**c**; P5, $n = 4$; P14, $n = 9$), (**f**; P5 and P14, $n = 4$) (**i**; P5, $n = 4$; P14, $n = 6$). Symbols represent individual mice. Three sections per mouse were quantified (mean ± s.e.m.). Scale bars, 50 µm. ND, not detected. **j**, Overview of the experimental set-up. **k**, Immunofluorescence images of anti-GFP (aGFP; green) or RFP (red) and CD206 (cyan) signals combined with Col IV (blue) from *Mrc1*$^{CreERT2/+}$*R26*$^{Confetti/+}$ mice. Arrowheads indicate confetti-negative (blank white), anti-GFP$^+$ (filled white) or RFP$^+$ (filled yellow) CD206$^+$ perivascular macrophages. Images are representative of three (P14) or four (P28) mice. Scale bars, 100 µm (main images); 25 µm (insets). **l**, Perivascular macrophage clone size distribution of $n = 46$ clones at P14 and $n = 42$ clones at P28. Data are pooled from three (P14) or four (P28) mice.

in EMPs, A1 cells or subsets of HSCs, whereas A2 cells and their microglia and CAM progeny were labelled (Extended Data Fig. 5g–o). When *Mrc1*$^{CreERT2/CreERT2}$*R26*$^{tdT/tdT}$ mice were pulsed with TAM at P14 and P16, only CAMs—and not microglia—were labelled with tdT (Extended Data Fig. 5p, q), suggesting that the segregation of CAMs and microglia is already completed during early postnatal development. These results indicate that CAMs and microglia share a common CD206$^+$ yolk sac progenitor and that the determination of cell fate occurs subsequently and locally in the developing CNS.

Meningeal origin of perivascular CAMs

Even though perivascular macrophages only establish in their specific niche after birth, they were shown to be originally derived from yolk sac progenitors[11,33]. Consistently, HSC-derived cells in *Cxcr4*^{creERT2}*R26*^{tdT} mice did not give rise to perivascular macrophages at P14 (Extended Data Fig. 6a–c), suggesting that the precursors of perivascular macrophages are independent of postnatal HSCs and temporarily reside in a different niche before they finally distribute in the perivascular space. A previous report has described *Mrc1*-expressing microglia in the embryonic brain parenchyma[21], raising the possibility that embryonic microglia could act as precursors of perivascular macrophages. To test this, we injected *Hexb*$^{CreERT2/CreERT2}$*R26*$^{YFP/YFP}$ pregnant female mice with 4OH-TAM at E16.5 (Fig. 3a) to induce YFP expression in fetal microglia, with no recombination in blood monocytes (Fig. 3b). We subsequently observed many YFP$^+$IBA1$^+$ microglia, but perivascular macrophages and meningeal macrophages were negative for YFP (Fig. 3c), suggesting that embryonic microglia do not contribute to perivascular macrophages. Additional experiments with different TAM protocols led to the same conclusion (Extended Data Fig. 6d–f).

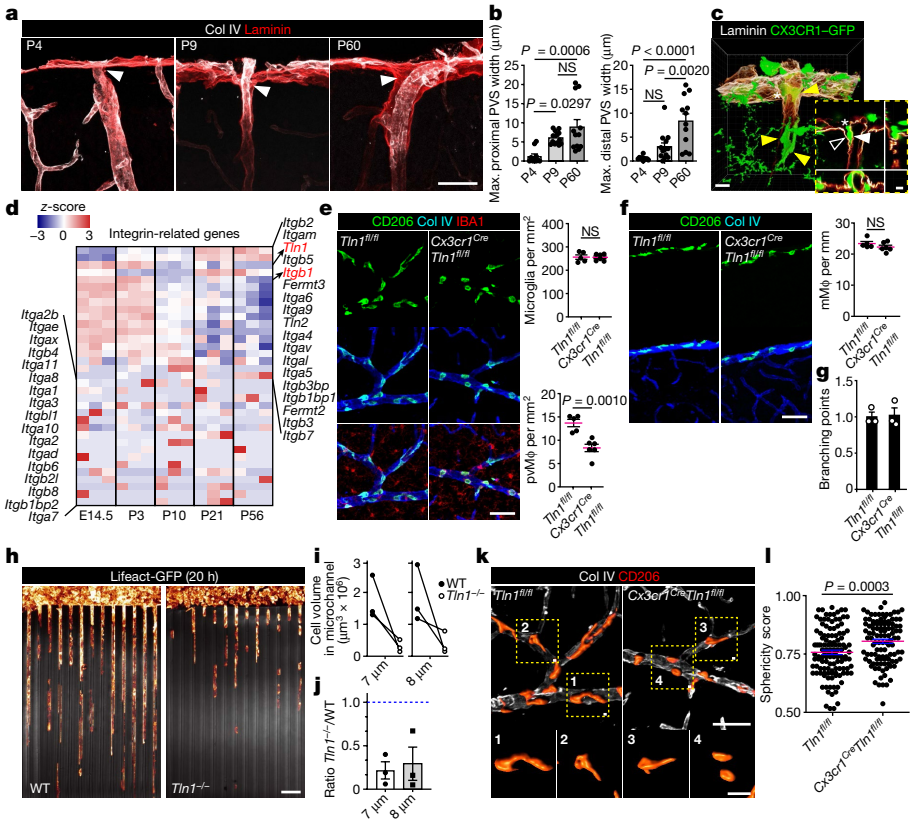

Fig. 4 | Establishment of perivascular macrophages after birth depends on intact integrin signalling. a, Cortical blood vessels in *Cx3cr1*$^{GFP/+}$ mice. Arrowheads indicate PVS enclosed by laminin$^+$ (red) and Col IV$^+$ (white) basal laminas. Representative of $n = 3$ mice per time point. Scale bar, 50 μm. **b**, Proximal (pial surface) or distal (50 μm depth) PVS width in *Cx3cr1*$^{GFP/+}$ mice. Symbols represent individual vessels (P4, $n = 10$; P9, $n = 13$; P60, $n = 12$; mean ± s.e.m.). Pooled from three mice per time point. One-way ANOVA with Tukey's multiple comparisons test. NS, not significant. **c**, Laminin$^+$ (white glow) cortical vessel with perivascular macrophages (yellow arrowheads) in P9 *Cx3cr1*$^{GFP/+}$ mice. Arrowheads depict outer (blank white) and inner (filled white) PVS basal laminas. Asterisk: perivascular macrophage entering the PVS. Image representative of three mice. Scale bars, 10 μm (main image); 5 μm (inset). **d**, Gene expression in CD206$^+$ meningeal macrophages. Arrows indicate genes chosen for further analysis (red). $n = 3$ replicates per time point. **e**, **f**, Immunofluorescence of IBA1$^+$ (red) microglia and CD206$^+$ (green) perivascular macrophages (**e**) or CD206$^+$ meningeal macrophages (**f**), with Col IV$^+$ (blue) at P14 and quantification (right). Three sections per mouse (*Tln1*$^{fl/fl}$, $n = 5$; *Cx3cr1*^{Cre}*Tln1*$^{fl/fl}$, $n = 6$) were quantified (mean ± s.e.m.). Two-sided unpaired *t*-test. Scale bars, 50 μm. **g**, Cortical vessel branch points in *Tln1*$^{fl/fl}$ and *Cx3cr1*^{Cre}*Tln1*$^{fl/fl}$ mice at P14 ($n = 3$ mice). Three sections per mouse were quantified (mean ± s.e.m.). **h**, Lifeact-GFP$^+$ wild-type and *Tln1*$^{-/-}$ bone-marrow-derived macrophages (BMDMs) in 8-μm microchannels (three independent experiments). Scale bar, 50 μm. **i**, **j**, Total BMDM volume (**i**) and ratio of cell volume (**j**). (Paired) symbols represent independent experiments ($n = 3$, mean ± s.e.m). **k**, Three-dimensional reconstruction of perivascular macrophages shown in **e**. Images are representative of four mice. Scale bars, 50 μm (main image); 20 μm (inset). **l**, Sphericity score of cortical *Tln1*$^{fl/fl}$ ($n = 120$) and *Cx3cr1*^{Cre}*Tln1*$^{fl/fl}$ ($n = 108$) perivascular macrophages at P14 (mean ± s.e.m.). Pooled from five (*Tln1*$^{fl/fl}$) or six (*Cx3cr1*^{Cre}*Tln1*$^{fl/fl}$) mice. Two-sided unpaired *t*-test.

We next examined meningeal macrophages as a potential source for the perivascular macrophage pool, as both cell types exhibit similar gene signatures in adulthood[1,11,17,19]. After injecting 4OH-TAM into pregnant *Mrc1*$^{CreERT2/CreERT2}$*R26*$^{tdT/tdT}$ mice at E16.5, all offspring were analysed at postnatal time points (Fig. 3d). No recombination was evident in blood monocytes (Fig. 3e), whereas almost all CD206$^+$meningeal macrophages were labelled with tdT (Fig. 3f). tdT$^+$CD206$^+$perivascular macrophages were not detectable at P5, at which time point perivascular macrophages per se are absent (Fig. 1c). Less than a third of microglia were tdT$^+$ at P5 and P14 (Fig. 3f). The percentage of tdT-expressing CD206$^+$perivascular macrophages was similar to that of CD206$^+$meningeal macrophages at P14 (Fig. 3f). These findings were confirmed using *Lyve1*$^{CreERT2/CreERT2}$*R26*$^{tdT/tdT}$ mice, in which robust labelling of meningeal macrophages at P5 and subsequent labelling of perivascular macrophages at P14 was evident, without affecting blood monocytes (Fig. 3g–i). We next investigated whether the perivascular spaces are populated by the clonal expansion of single perivascular macrophages or through a continuous infiltration of meningeal macrophages. We thus generated *Mrc1*$^{CreERT2/+}$*R26*$^{Confetti/+}$ mice, which undergo a stochastic recombination and expression of either of the four fluorescent proteins after injection of TAM[17,34] (Fig. 3j). We observed perivascular macrophage clones of various sizes when recombination was induced at P1. Simultaneously, single vessels were often occupied by several different-coloured clones. By contrast, induction at P14 generated mostly isolated *Confetti*$^+$ perivascular macrophages (Fig. 3k, l). These data strongly suggest that during early postnatal development, perivascular macrophages expand by two mechanisms—local proliferation together with continuous infiltration of meningeal macrophages. The postnatal expansion of perivascular macrophages, meningeal macrophages and microglia was found to depend on *Irf8* and *Mafb* (Extended Data Fig. 6g–r), which are developmentally regulated (Extended Data Fig. 3d).

Together, we conclude that developing leptomeninges serve as an intermediate environmental niche, from which meningeal macrophages presumably migrate into the perivascular space to give rise to perivascular macrophages after birth when the perivascular niche develops.

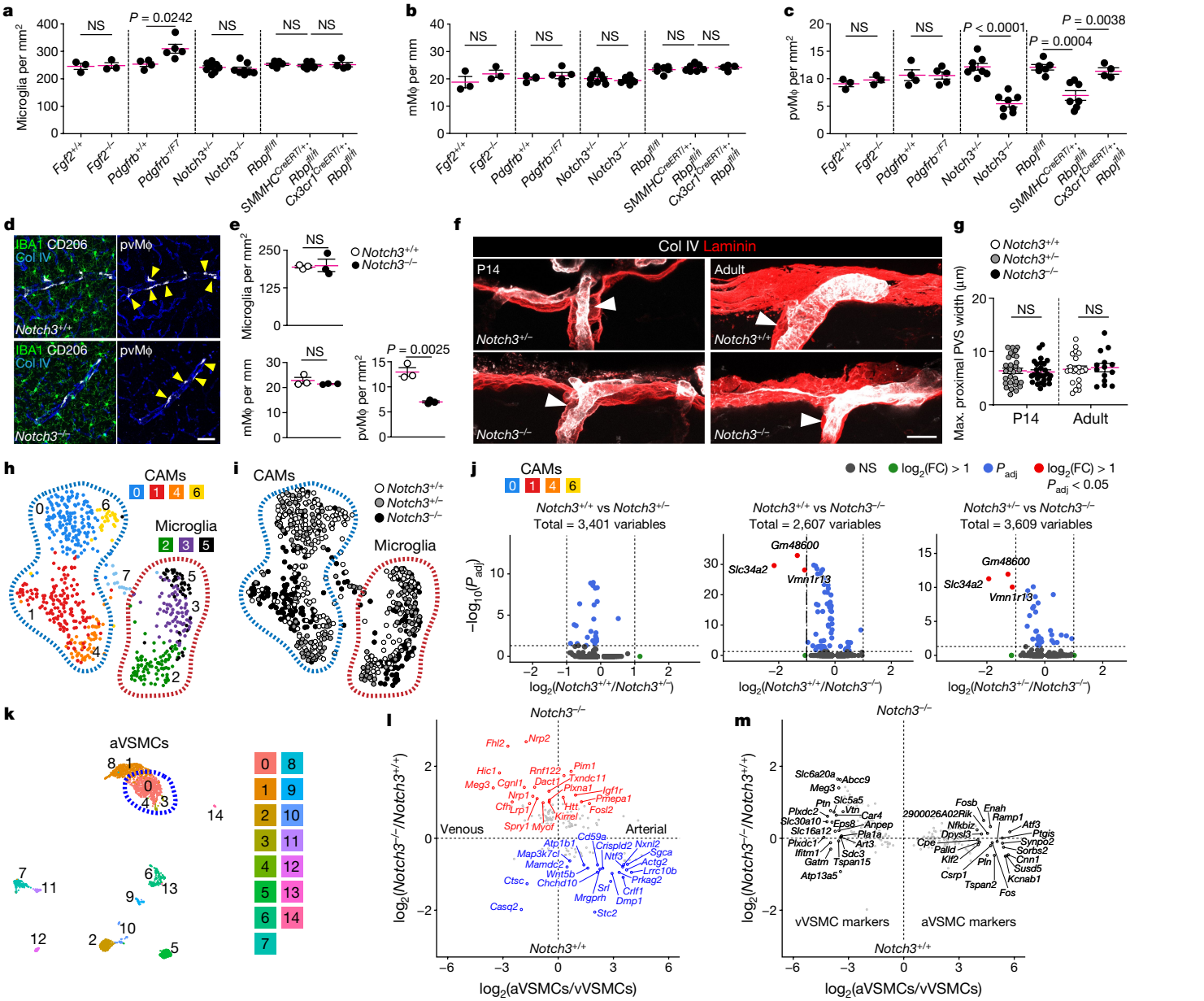

Fig. 5 | Formation of perivascular macrophages requires arterial vascular smooth muscle cells. a–**c**, Quantification of cortical microglia (**a**), meningeal macrophages (**b**) and perivascular macrophages (**c**) in *Fgf2*$^{+/+}$ ($n = 3$), *Fgf2*$^{-/-}$ ($n = 3$), *Pdgfrb*$^{+/+}$ ($n = 4$), *Pdgfrb*$^{-/F7}$ ($n = 5$), *Notch3*$^{+/-}$ ($n = 8$), *Notch3*$^{-/-}$ ($n = 8$), *Rbpj*$^{fl/fl}$ ($n = 6$), *SMMHC*^{CreERT2}*Rbpj*$^{fl/fl}$ ($n = 7$) and *Cx3cr1*^{CreERT2}*Rbpj*$^{fl/fl}$ ($n = 4$) mice at P14. Two-sided unpaired *t*-test (*Fgf2*, *Pdgfrb*, *Notch3*) or one-way ANOVA with Tukey's multiple comparisons test (*Rbpj*). **d**, IBA1 (green), CD206 (white) and Col IV^{+} (blue) immunofluorescence in the adult mouse cortex ($n = 3$ for *Notch3*$^{+/+}$ and *Notch3*$^{-/-}$). Arrowheads indicate perivascular macrophages. Scale bar, 50 μm. **e**, Quantification of microglia, meningeal macrophages and perivascular macrophages. Symbols represent individual mice ($n = 3$, mean ± s.e.m.). Three sections per mouse were quantified. Two-sided unpaired *t*-test. **f**, **g**, Arrowheads indicate PVS around cortical vessels (**f**). Scale bar, 50 μm. Width of the PVS (**g**). Symbols represent individual vessels (*Notch3*$^{+/-}$, $n = 29$; *Notch3*$^{+/+}$, $n = 21$; *Notch3*$^{-/-}$, P14, $n = 28$; adult $n = 14$; mean ± s.e.m.). Pooled from four (P14 *Notch3*$^{+/+}$, *Notch3*$^{+/-}$) or three (adult *Notch3*$^{+/+}$, *Notch3*$^{-/-}$) mice. Two-sided unpaired *t*-test. **h**, UMAP of 629 microglia and CAMs from *Notch3*$^{+/+}$, *Notch3*$^{+/-}$ or *Notch3*$^{-/-}$ mice at P14. **i**, Genotype-distribution plotted on UMAP. **j**, Volcano plots comparing gene expression of pooled CAMs between genotypes. The −log$_{10}$-transformed adjusted *P* value (*P* adj, *y* axis) was plotted against the log$_2$-transformed fold change in expression between the genotypes (*x* axis). **k**, UMAP of 2,254 mural cells from the brains of adult *Notch3*$^{+/+}$*Tagln*^{CreERT2}*R26*^{tdT} or *Notch3*$^{-/-}$*Tagln*^{CreERT2}*R26*^{tdT} mice. Dotted line: arterial VSMC (aVSMC) clusters. **l**, Differential gene expression in aVSMCs between *Notch3*$^{+/+}$ and *Notch3*$^{-/-}$ (*y* axis) was plotted against the log-transformed fold change in expression between aVSMCs and venous (v) VSMCs (*x* axis; as determined previously[25]). Red, top 20 upregulated genes; blue, top 20 downregulated genes. **m**, Top 100 vVSMC (left) and aVSMC (right) marker genes. The *x* and *y* axes are as in **l**. The top 20 markers are annotated.

Niche occupation is integrin-dependent

High-resolution confocal and electron microscopy revealed a time-dependent dynamic establishment and gradual expansion of the Virchow–Robin space (Fig. 4a–c, Extended Data Fig. 7a), which allows meningeal macrophages to descend to the developing perivascular niche. Orchestrated cell movement can be mediated by signalling from adhesion receptors—such as integrins—interacting with the extracellular environment[35]. Of note, bulk RNA-seq data revealed an age-dependent regulation in the expression levels of several integrins

in meningeal macrophages (Fig. 4d). As perivascular macrophages are only established in the early postnatal period, we focused on P3, which was characterized by high expression of genes including *Tln1* (Talin-1) and *Itgb1* (integrin subunit beta 1). Talin-1 is a cytosolic adaptor protein that controls the activation of integrin-mediated signalling pathways[36]. In the brains of $Cx3cr1^{Cre/+}Tln1^{fl/fl}$ mice, in which *Tln1* is deleted in brain myeloid cells including microglia and CAMs, the density of microglia and meningeal macrophages was comparable to control $Tln1^{fl/fl}$ littermates, whereas perivascular macrophages were decreased (Fig. 4e, f). *Tln1* deficiency did not affect the prenatal distribution of microglia and meningeal macrophages in the embryonic brain (Extended Data Fig. 7b, c), the number of vessel branching points, or parameters of vascular integrity (Fig. 4g, Extended Data Fig. 7d, e), which excludes impaired vascularization as a possible explanation for the reduction of perivascular macrophages in $Cx3cr1^{Cre/+}Tln1^{fl/fl}$ mice. Mechanistically, *Tln1*-deficient macrophages were impaired in migrating into in vitro microchannels of a similar diameter to the perivascular space (Fig. 4b, h–j). Three-dimensional reconstructions revealed that perivascular macrophages in $Cx3cr1^{Cre}Tln1^{fl/fl}$ mice had a more roundish morphology than controls (Fig. 4k, l). On the other hand, $Vav^{Cre/+}Itgb1^{fl/fl}$ mice, in which all haematopoietic cells lack *Itgb1*, showed only subtle changes in the numbers of perivascular macrophages, microglia and meningeal macrophages (Extended Data Fig. 7f, g), suggesting a redundant role of *Itgb1*. Overall, these results indicate that perivascular macrophages are evolving after birth in the developing Virchow–Robin space in an integrin-dependent manner, although the molecular mechanisms are yet to be fully resolved.

Vascular smooth muscle cells are key

The vasculature of the brain is a complex structure that consists of multiple cell types including endothelial cells, astrocytes and mural cells, such as pericytes or VSMCs[37]. To test which cell types contribute to the establishment of perivascular macrophages during development, we first used mice that lack fibroblast growth factor 2 ($Fgf2^{-/-}$), in which astrocyte differentiation is impaired during early postnatal stages[38]. Given that astrocytic endfeet develop mostly at perinatal stages[39], we hypothesized that astrocyte impairments could affect the distribution of perivascular macrophages. In $Fgf2^{-/-}$ mice, however, the numbers of perivascular macrophages, microglia and meningeal macrophages were comparable to those in $Fgf2^{+/+}$ control mice at P14 (Fig. 5a–c, Extended Data Fig. 8a, b). We next analysed platelet-derived growth factor receptor β mutant mice ($Pdgfrb^{-/F7}$), which show pericyte hypoplasia in the developing brain[40]. The density of microglia in $Pdgfrb^{-/F7}$ mice was significantly increased compared to $Pdgfrb^{+/+}$ controls through a reactive gliosis of $P2RY12^{+}$ microglia (Fig. 5a, Extended Data Fig. 8c–e), whereas the numbers of perivascular macrophages and meningeal macrophages did not differ between the genotypes (Fig. 5b, c, Extended Data Fig. 8c, d). As perivascular macrophages are predominantly localized in the Virchow–Robin space of arteries and arterioles that contain VSMCs, arterial VSMCs could have a functional role in determining the proper distribution of perivascular macrophages. We therefore used mice that lack *Notch3*, which controls the development and homeostasis of arterial VSMCs[41,42]. Indeed, VSMCs were strongly reduced in the arteries and arterioles of $Notch3^{-/-}$ brains (Extended Data Fig. 8f–i), as described before[43]. Notably, the number of perivascular macrophages—but not that of microglia and meningeal macrophages—was strongly reduced in $Notch3^{-/-}$ mice compared to $Notch3^{+/-}$ littermate controls (Fig. 5a–c, Extended Data Fig. 8f–i). We further investigated cell-type-specific roles of Notch signalling using mice carrying a floxed version of the *Rbpj* gene[44], which encodes recombination signal binding protein for immunoglobulin kappa J region (RBPJ)—a major downstream transcription factor of the Notch pathway. Crossing $Rbpj^{fl/fl}$ mice with $SMMHC^{CreERT2}$ mice was followed by injection of TAM, which allowed for the specific deletion of *Rbpj* from arterial VSMCs[45]. This intervention led to impaired development of VSMCs, with similarities to $Notch3^{-/-}$ mice[46] (Extended Data Fig. 8j–o), and a reduction in the number of perivascular macrophages, whereas microglia and meningeal macrophages were unaffected (Fig. 5a–c, Extended Data Fig. 8j–m). A myeloid-cell-intrinsic role of Notch signalling for the establishment of perivascular macrophages was excluded as the numbers of perivascular macrophages, microglia and meningeal macrophages were unaffected in $Cx3cr1^{CreERT2}Rbpj^{fl/fl}$ mice (Fig. 5a–c, Extended Data Fig. 8n, o). This is in line with our observation that none of the CNS macrophage populations expressed *Notch3* (Extended Data Fig. 3e). Together, our results suggest that the presence of arterial VSMCs is crucial for the proper distribution of perivascular macrophages during development.

Loss of *Notch3* induces venous shift

Finally, we asked which *Notch3*-associated signals modulate the postnatal formation of perivascular macrophages. Adult $Notch3^{-/-}$ mice showed a reduction of perivascular macrophages as compared to $Notch3^{+/+}$ mice, whereas no differences were observed for their rates of proliferation ($Ki\text{-}67^{+}$) or apoptosis (cleaved caspase 3^{+}) (Fig. 5d, e, Extended Data Fig. 8p, q). No apparent changes of the proximal perivascular spaces were detected, which indicates that the spatial anatomical preconditions for proper perivascular macrophage seeding were unaltered in *Notch3*-deficient mice (Fig. 5f, g). We next intensively profiled CAMs and microglia from *Notch3*-deficient and control mice by scRNA-seq[47] (Extended Data Fig. 9a). Clustering revealed five microglia and CAM clusters (C0, C2, C3, C9 and C12) and clusters for contaminating brain cells (other clusters) (Extended Data Fig. 9b–f). A focused re-analysis of CAMs that lack *Notch3* revealed only subtle variations of single genes, suggesting non-cell-autonomous effects of this mutation (Fig. 5h–j, Extended Data Fig. 9g–j). By contrast, arterial VSMCs (clusters C0, C3 and C4) isolated from $Notch3^{+/+}Tagln^{CreERT2}R26^{tdT}$ or $Notch3^{-/-}Tagln^{CreERT2}R26^{tdT}$ mice showed major transcriptional differences (Fig. 5k, Extended Data Fig. 9k, l). Although characteristic genes of the arterial VSMC contractile machinery—such as *Myh11*, *Atf3*, *Acta2* and *Tagln*—were not affected, we observed a pronounced but incomplete arterial-to-venous-shift in the transcriptomic profile of arterial VSMCs, with lower expression of arterial genes such as *Stc2* or *Crlf1* and concomitantly increased levels of venous genes such as *Nrp2* and *Fhl2* (ref. [25]) (Fig. 5l, m). Together, these results suggest that *Notch3* function in VSMCs is required for the establishment of perivascular macrophages, but is dispensable for the development of the perivascular space.

Discussion

In this study we have uncovered the ontogenetic trajectory, distribution, kinetics and gene expression profiles of defined subsets of CAMs, as well as crucial intercellular communications and molecular machineries. Using scRNA-seq, we identified a distinct *Mrc1* $(CD206)^{+}$ subset within the A2 pre-macrophage population. A previous study described a similar $CD206^{+}$ yolk sac population and suggested that these cells were committed progenitors of CAMs, distinct from the microglia ancestry[33]. However, our fate-mapping analysis with the $Mrc1^{CreERT2}$ mouse line revealed instead that $CD206^{+}$ yolk sac progenitors represent an intermediate state of cells during embryogenesis that can give rise to all types of CNS macrophages, confirming their ontogenetic resemblance (Extended Data Fig. 10). Furthermore, our present data indicate that the definitive specification of CNS macrophage populations is accomplished by a stepwise program at perinatal stages within their anatomical CNS niche and is seemingly imprinted by local cues.

The establishment of perivascular macrophages requires the presence of arterial VSMCs and integrin signalling. Single-cell profiling of vessel-associated cells in mice that lack *Notch3* revealed that CAMs and microglia were basically unaltered, whereas arterial VSMCs exhibited a changed transcriptomic pattern, with an arterial-to-venous-shift, as

observed previously[43]. Therefore, the reduced number of perivascular macrophages in *Notch3*-deficient mice might also be related to the loss of arterial identity rather than being a result of the loss of arterial VSMCs—a possibility that should be considered in future experiments.

Together, our analysis sheds light on the ontogeny and specification of CNS macrophages within their specific tissue niches. As the behaviour and functions of CAMs during normal CNS development, steady state and disease are still poorly defined, our *Mrc1*-based mouse tool to specifically target CAMs will help to elucidate CAM biology. This may open new avenues for a better understanding of CNS development and disease.

Online content

Any methods, additional references, Nature Research reporting summaries, source data, extended data, supplementary information, acknowledgements, peer review information; details of author contributions and competing interests; and statements of data and code availability are available at https://doi.org/10.1038/s41586-022-04596-2.

1. Van Hove, H. et al. A single-cell atlas of mouse brain macrophages reveals unique transcriptional identities shaped by ontogeny and tissue environment. *Nat. Neurosci.* **22**, 1021–1035 (2019).
2. Kierdorf, K., Masuda, T., Jordao, M. J. C. & Prinz, M. Macrophages at CNS interfaces: ontogeny and function in health and disease. *Nat. Rev. Neurosci.* **20**, 547–562 (2019).
3. Herz, J., Filiano, A. J., Smith, A., Yogev, N. & Kipnis, J. Myeloid cells in the central nervous system. *Immunity* **46**, 943–956 (2017).
4. Prinz, M., Jung, S. & Priller, J. Microglia biology: one century of evolving concepts. *Cell* **179**, 292–311 (2019).
5. Prinz, M., Erny, D. & Hagemeyer, N. Ontogeny and homeostasis of CNS myeloid cells. *Nat. Immunol.* **18**, 385–392 (2017).
6. Colonna, M. & Butovsky, O. Microglia function in the central nervous system during health and neurodegeneration. *Annu. Rev. Immunol.* **35**, 441–468 (2017).
7. Prinz, M., Masuda, T., Wheeler, M. A. & Quintana, F. J. Microglia and central nervous system-associated macrophages-from origin to disease modulation. *Annu. Rev. Immunol.* **39**, 251–277 (2021).
8. Santisteban, M. M. et al. Endothelium–macrophage crosstalk mediates blood–brain barrier dysfunction in hypertension. *Hypertension* **76**, 795–807 (2020).
9. Faraco, G. et al. Perivascular macrophages mediate the neurovascular and cognitive dysfunction associated with hypertension. *J. Clin. Invest.* **126**, 4674–4689 (2016).
10. Pires, P. W. et al. Improvement in middle cerebral artery structure and endothelial function in stroke-prone spontaneously hypertensive rats after macrophage depletion. *Microcirculation* **20**, 650–661 (2013).
11. Goldmann, T. et al. Origin, fate and dynamics of macrophages at central nervous system interfaces. *Nat. Immunol.* **17**, 797–805 (2016).
12. Gomez Perdiguero, E. et al. Tissue-resident macrophages originate from yolk-sac-derived erythro-myeloid progenitors. *Nature* **518**, 547–551 (2015).
13. Kierdorf, K. et al. Microglia emerge from erythromyeloid precursors via Pu.1- and Irf8-dependent pathways. *Nat. Neurosci.* **16**, 273–280 (2013).
14. Ginhoux, F. & Guilliams, M. Tissue-resident macrophage ontogeny and homeostasis. *Immunity* **44**, 439–449 (2016).
15. Ginhoux, F. et al. Fate mapping analysis reveals that adult microglia derive from primitive macrophages. *Science* **330**, 841–845 (2010).
16. Hagemeyer, N. et al. Transcriptome-based profiling of yolk sac-derived macrophages reveals a role for Irf8 in macrophage maturation. *EMBO J.* **35**, 1730–1744 (2016).
17. Jordao, M. J. C. et al. Single-cell profiling identifies myeloid cell subsets with distinct fates during neuroinflammation. *Science* **363**, eaat7554 (2019).
18. Masuda, T. et al. Novel Hexb-based tools for studying microglia in the CNS. *Nat. Immunol.* **21**, 802–815 (2020).
19. Mrdjen, D. et al. High-dimensional single-cell mapping of central nervous system immune cells reveals distinct myeloid subsets in health, aging, and disease. *Immunity* **48**, 380–395 (2018).
20. Masuda, T. et al. Spatial and temporal heterogeneity of mouse and human microglia at single-cell resolution. *Nature* **566**, 388–392 (2019).
21. Hammond, T. R. et al. Single-cell RNA sequencing of microglia throughout the mouse lifespan and in the injured brain reveals complex cell-state changes. *Immunity* **50**, 253–271 (2019).
22. Dasgupta, K. & Jeong, J. Developmental biology of the meninges. *Genesis* **57**, e23288 (2019).
23. Munro, D. A. D. et al. CNS macrophages differentially rely on an intronic Csf1r enhancer for their development. *Development* **147**, dev194449 (2020).
24. Zhao, Z., Nelson, A. R., Betsholtz, C. & Zlokovic, B. V. Establishment and dysfunction of the blood–brain barrier. *Cell* **163**, 1064–1078 (2015).
25. Vanlandewijck, M. et al. A molecular atlas of cell types and zonation in the brain vasculature. *Nature* **554**, 475–480 (2018).
26. Langen, U. H., Ayloo, S. & Gu, C. Development and cell biology of the blood–brain barrier. *Annu. Rev. Cell Dev. Biol.* **35**, 591–613 (2019).
27. Corada, M. et al. Sox17 is indispensable for acquisition and maintenance of arterial identity. *Nat. Commun.* **4**, 2609 (2013).
28. Zahr, A. et al. Endomucin prevents leukocyte-endothelial cell adhesion and has a critical role under resting and inflammatory conditions. *Nat. Commun.* **7**, 10363 (2016).
29. Werner, Y. et al. Cxcr4 distinguishes HSC-derived monocytes from microglia and reveals monocyte immune responses to experimental stroke. *Nat. Neurosci.* **23**, 351–362 (2020).
30. Ydens, E. et al. Profiling peripheral nerve macrophages reveals two macrophage subsets with distinct localization, transcriptome and response to injury. *Nat. Neurosci.* **23**, 676–689 (2020).
31. Bertrand, J. Y. et al. Three pathways to mature macrophages in the early mouse yolk sac. *Blood* **106**, 3004–3011 (2005).
32. Butler, A., Hoffman, P., Smibert, P., Papalexi, E. & Satija, R. Integrating single-cell transcriptomic data across different conditions, technologies, and species. *Nat. Biotechnol.* **36**, 411–420 (2018).
33. Utz, S. G. et al. Early fate defines microglia and non-parenchymal brain macrophage development. *Cell* **181**, 557–573 (2020).
34. Tay, T. L. et al. A new fate mapping system reveals context-dependent random or clonal expansion of microglia. *Nat. Neurosci.* **20**, 793–803 (2017).
35. Michael, M. & Parsons, M. New perspectives on integrin-dependent adhesions. *Curr. Opin. Cell Biol.* **63**, 31–37 (2020).
36. Calderwood, D. A., Campbell, I. D. & Critchley, D. R. Talins and kindlins: partners in integrin-mediated adhesion. *Nat. Rev. Mol. Cell Biol.* **14**, 503–517 (2013).
37. Mastorakos, P. & McGavern, D. The anatomy and immunology of vasculature in the central nervous system. *Sci. Immunol.* **4**, eaav0492 (2019).
38. Irmady, K., Zechel, S. & Unsicker, K. Fibroblast growth factor 2 regulates astrocyte differentiation in a region-specific manner in the hindbrain. *Glia* **59**, 708–719 (2011).
39. Shoneye, T. et al. Differential proliferation and maturation of subcortical astrocytes during postnatal development. *Front. Neurosci.* **14**, 435 (2020).
40. Daneman, R., Zhou, L., Kebede, A. A. & Barres, B. A. Pericytes are required for blood–brain barrier integrity during embryogenesis. *Nature* **468**, 562–566 (2010).
41. Wang, Q., Zhao, N., Kennard, S. & Lilly, B. Notch2 and Notch3 function together to regulate vascular smooth muscle development. *PLoS ONE* **7**, e37365 (2012).
42. Henshall, T. L. et al. Notch3 is necessary for blood vessel integrity in the central nervous system. *Arterioscler. Thromb. Vasc. Biol.* **35**, 409–420 (2015).
43. Domenga, V. et al. Notch3 is required for arterial identity and maturation of vascular smooth muscle cells. *Genes Dev.* **18**, 2730–2735 (2004).
44. Han, H. et al. Inducible gene knockout of transcription factor recombination signal binding protein-J reveals its essential role in T versus B lineage decision. *Int. Immunol.* **14**, 637–645 (2002).
45. Wirth, A. et al. G_{12}-G_{13}–LARG-mediated signaling in vascular smooth muscle is required for salt-induced hypertension. *Nat. Med.* **14**, 64–68 (2008).
46. Fouillade, C. et al. Transcriptome analysis for Notch3 target genes identifies Grip2 as a novel regulator of myogenic response in the cerebrovasculature. *Arterioscler. Thromb. Vasc. Biol.* **33**, 76–86 (2013).

Methods

Mice

C57BL/6N mice were used as wild-type mice. Transgenic lines including *Cx3cr1*^{GFP} (B6.129P2(Cg)-*Cx3cr1*^{tm1Litt}/J), *Cx3cr1*^{Cre} (B6J.B6N(Cg)-*Cx3cr1*$^{tm1.1(cre)Jung}$/J), *Cx3cr1*^{CreERT2} (B6.129P2(C)-*Cx3cr1*$^{tm2.1(cre/ERT2)Jung}$/J), *Hexb*^{CreERT2} (ref. [18]), *Cxcr4*$^{CreERT2\text{-}Ires\text{-}YFP}$ (*Cxcr4*^{CreERT2})[29], *SMMHC*^{CreERT2} (B6.FVB-Tg(Myh11-cre/ERT2)1Soff/J), *Vav*^{Cre} (ref. [48]), *Tln1*^{fl} (ref. [49]), *Fgf2*$^{-/-}$ (ref. [50]), *Pdgfrb*$^{-/F7}$ (ref. [40]), *Notch3*$^{-/-}$ (refs. [43,51]), *Rbpj*^{fl} (ref. [44]), *Itgb1*^{fl} (ref. [52]), *Irf8*^{fl} (ref. [53]), *R26*^{tdT} (Jackson Laboratory, 007914), *R26*^{YFP} (Jackson Laboratory, 006148), *R26*^{Confetti} (ref. [54]), *Lyve1*^{CreERT2} (B6/JGpt- Lyve1-CreERT2, GemPharmatech) and *Tagln*$^{tm1(cre/ERT2)Feil}$ mice (both genders) were used in this study. *Rbpj*^{fl} mice were provided by Riken (RBRC01071). *Mafb*^{fl} mice[55] were provided by L. Goodrich, President and Fellows of Harvard College. Mice were bred in-house under pathogen-free conditions. No statistical method was used to predetermine sample size. Blinding and randomization were not used in this study. All animal experiments were approved by local administration and were performed in accordance with the respective national and federal regulations. All animal experiments were approved by the Regierungspräsidium Freiburg, Germany, or were conducted according to relevant national and international guidelines contained in the 'Act on Welfare and Management of Animals' (Ministry of Environment of Japan) and 'Regulation of Laboratory Animals' (Kyushu University) and under the protocols approved by the Institutional Animal Care and Use committee review panels at Kyushu University. Immunohistochemistry on human samples with no reported pathology (including male and female individuals) was conducted in accordance with the institutional review board of the University of Freiburg Medical Center (approval number 10008/09).

Generation of *Mrc1*^{CreERT2} mice

The CRISPR–Cas9 system was used to knock-in the T2A-CreERT2 cassette into the *Mrc1* locus by injecting mouse embryos on a C57Bl/6N background with in-vitro-assembled CRISPR–Cas9 constructs in combination with donor DNA generated by gene synthesis (GenScript). In both cases, double-strand break was directed using a single-guide RNA (sgRNA; sequence 5′- CCUUUAUACACAGGAUACUGUAA′), which was tested by transient transfection of NIH3t3 cells followed by surveyor assays. For the donor vector for the *Mrc1*^{CreERT2} mouse line the sequence encoding CreERT2 preceded by the sequence encoding a T2A self cleavage peptide was flanked by a 680-bp 5´and a 800-bp 3´homology region. Precise sequences for the HDR donor vectors are available upon request. Correct integration of the T2A-CreERT2 cassette upstream of the *Mrc1* stop codon (Extended Data Fig. 4a) was confirmed by diagnostic PCR. Sequencing of the genomic region of interest after amplification by PCR was further used to verify correct integration. After germline transmission, correctly targeted founders were crossed with C57Bl/6N mice to establish the colonies for this study.

Tamoxifen treatment

For activation of Cre recombinase, tamoxifen (TAM, Sigma-Aldrich), or 4-hydroxytamoxifen (4OH-TAM, Sigma-Aldrich) together with progesterone (Sigma-Aldrich) was dissolved in corn oil (Sigma-Aldrich) before injection. To induce Cre recombination in embryos, pregnant females were intraperitoneally injected with 4OH-TAM (75 mg per kg body weight) with progesterone (37.5 mg per kg body weight) at E9.0 (Fig. 2h–k), E9.5 (Extended Data Figs. 2e–g, 5g, i, k, m) or E16.5 (Fig. 3, Extended Data Fig. 5g, n, o). To induce Cre recombination in neonates, pups were intraperitoneally injected with 0.1 mg TAM per 5 µl oil at P1 (Fig. 3j) or P1 and P3 (Fig. 5, Extended Data Figs. 6, 9b–e) or with 0.4 mg TAM per 20 µl at P14 and P16 (Extended Data Fig. 5p, q). In 6–10-week old adult mice, Cre recombination was induced by injecting 1 mg TAM per 100 µl oil intraperitoneally for 5 consecutive days (Extended Data Fig. 2h–k), or 4 mg TAM per 200 µl oil intraperitoneally twice 48 h apart (Extended Data Fig. 4i–l).

scRNA-seq

A1/A2 cells were sorted by fluorescence-activated cell sorting (FACS) from the extra-embryonic yolk sac at E9.5 into a 384-well (Bio-Rad Laboratories) plate containing lysis buffer and barcodes. The gating strategies for FACS sorting, related to the datasets shown in Fig. 2a–d, Extended Data Fig. 5b–d, are shown in Extended Data Fig. 5a. RNA amplification and library preparation was performed using an automated and miniaturized CEL-Seq2 protocol on a mosquito nanolitre-scale liquid-handling robot[56,57]. Eight libraries with 192 cells each were sequenced per lane on an Illumina HiSeq 3000 sequencing system (Control Software v.2.0.2, paired-end multiplexing run) at a depth of around 130,000–200,000 reads per cell. Transcriptome alignment of paired end reads was conducted using bwa (v.0.6.2-r126) with default parameters[58]. All isoforms of the same gene were treated as a single gene locus. The right mate of each read pair was mapped to the ensemble of all gene loci and to the set of 92 ERCC spike-ins in sense direction[59]. Reads mapping to multiple loci were discarded. The left read contains the barcode information: the first six bases represented the unique molecular identifier (UMI), followed by six bases with the cell-specific barcode. A polyT stretch formed the remainder of the left read and was not used for quantification. The number of UMIs per transcript was aggregated for each gene locus and assigned to individual cells depending on the barcode. Binomial statistics were used to model transcript counts from the number of observed UMIs leading to non-integer values in the associated counts tables[60]. Further analysis and data normalization were performed using the Seurat package as previously described[32]. The scRNA seq SmartSeq2 data shown in Fig. 5h–j were generated following the original publication[61] with the following specifications: 0.0025 µl of a 1:40,000 diluted ERCC spike-in (Thermo Fisher Scientific) concentration stock was used, and all cDNA was amplified with 25 PCR cycles before quality control with a Bioanalyzer (Agilent Biosystems). The libraries were sequenced on a HiSeq3000 with single 50-bp reads (dual indexing reads). The sequencing and transcriptomic data were generated at the Single Cell Core Facility (SICOF) at the Karolinska Institute. Single-cell data generated with the Smart-Seq2 technology was aligned with STAR v.2.7.8a[62] to the mouse reference genome Gencode M26[63]. Cells with a high mitochondrial content, high spike-in content or low number of genes detected were discarded. Subsequent bioinformatics analyses, such as dimensionality reduction, clustering and visualization were performed with the Seurat toolkit. Volcano plots were generated with the R package EnhancedVolcano. For the Smart-Seq2 single-cell analysis of the *Notch3*$^{+/+}$*Tagln*^{CreERT2}*R26*^{tdT} and *Notch3*$^{-/-}$*Tagln*^{CreERT2}*R26*^{tdT} mice (Fig. 5k–m), the experiment and raw data processing were performed as previously described[25].

Bulk RNA-seq

Microglia and CAMs were FACS-sorted from whole brains of wild-type mice (see gating strategies used for FACS sorting shown in Supplementary Fig. 1) into a collection tube and then total RNA was extracted using a Picopure RNA extraction kit (Life Technologies) according to the manufacturer's protocol. The SMARTer Ultra Low Input RNA Kit for Sequencing v4 (Clontech Laboratories) was used to generate first strand cDNA from 150 to 600 pg total RNA. Double-stranded cDNA was amplified by long-distance PCR (12–14 cycles) and purified by magnetic bead clean-up. Library preparation was performed as described in the Illumina Nextera XT Sample Preparation Guide (Illumina). A total of 150 pg of input cDNA was tagmented (tagged and fragmented) by the Nextera XT transposome. The products were purified and amplified through a limited-cycle PCR program to generate multiplexed sequencing libraries. The libraries were quantified using the KAPA Library Quantification Kit (Illumina) and ABI Prism User Guide (Roche Sequencing Solutions). Equimolar amounts of each library were pooled, and the pools were used for cluster generation on the cBot with the Illumina TruSeq SR Cluster Kit v3. The sequencing run was performed either on a HiSeq 1000 instrument (Control Software v.2.2.68) using the indexed, 50 cycles single-read

protocol and the TruSeq SBS v3 Reagents according to the Illumina HiSeq 1000 System User Guide, or on a NextSeq 2000 instrument, (Control Software v.1.2.0.36376) using one 100 cycles P2 Flow Cell with the dual index, single-read run parameters. The resulting image analysis and base calling were done by Real Time Analysis (RTA) v.3.7.17 software, which resulted in .bcl files, which were converted into fastq files with bcl2fastq v.2.20 software. RNA isolation, library preparation and sequencing were performed at the Genomics Core Facility at KFB—Center of Excellence for Fluorescent Bioanalytics (University of Regensburg). Bulk RNA-seq data were aligned with STAR v.2.7.8a[62] to the mouse reference genome Gencode M26[63]. Counts were obtained using FeatureCounts v.2.0.2. Genes with sum count expression of less than 5 were filtered out. Differential expression was performed using the limma trend method[64] on the $\log_2$ counts per million (CPM) values. Heat maps and bar plots were generated with the R packages pheatmap and ggplot2, respectively.

Flow cytometry

After being removed from pregnant females, the extra-embryonic yolk sac was homogenized with syringes in HBSS containing 15 mM HEPES buffer and 0.54 % glucose. After spinning down, the pellet containing the yolk sac progenitors at the bottom of the tube was then collected and washed once with PBS containing 2 % FCS and 10 mM EDTA before staining. The single-cell suspension was used for the staining procedure as described[18]. Fc receptors were blocked with Fc Block (2.4G2, BD Biosciences, 1:250) for 10 min at 4 °C before incubation with the primary antibodies. Cells were stained with antibodies directed against CD11b (M1/70, BioLegend, 1:300), CD45 (30-F11, BD Biosciences or Thermo Fisher Scientific, 1:200), Ly6C (AL-21, BD Biosciences, 1:200), Ly6G (1A8, BD Biosciences or BioLegend, 1:300), Gr1 (RB6-8C5, BioLegend, 1:300), CD115 (AFS98, Thermo Fisher Scientific, 1:200), CD11c (N4A18, Thermo Fisher Scientific, 1:300), F4/80 (BM8, BioLegend, 1:200), CD3e (eBio500A2, Thermo Fisher Scientific, 1:300), CD19 (eBio1D3, Thermo Fisher Scientific, 1:200), CD206 (C068C2, BioLegend, 1:200), CD93 (AA4.1, BioLegend, 1:200), c-Kit/CD117 (2B8, BioLegend, 1:200), Sca1 (D7, BD Biosciences, 1:200), CD48 (HM48-1, BioLegend, 1:200) and CD150 (TC15-12F12.2, BioLegend, 1:200) for 45 min at 4 °C. After washing, cells were sorted using a MoFlo Astrios (Beckman Coulter) or analysed using a BD LSRFortessa (Becton Dickinson). Viable cells were gated by staining with Fixable Viability Dye (65-0866, eBioscience) or DAPI. Data were acquired with FACSDiva (Becton Dickinson). Post-acquisition analysis was performed using FlowJo v.10.5.3.

Macrophage invasion into microchannels

BMDMs were cultured by standard M-CSF culture over six days, as previously described[65]. Microchannels were custom-designed and of 7 µm or 8 µm width and 10 µm height (4Dcell). Microchannel experiments were performed according to the manufacturer's instructions with minor modifications. In brief, microchannel dishes were washed three times with 3 ml PBS for 5 min at room temperature. After this, microchannels were coated with 3 ml FCS for 1 h at 37 °C and then washed a further three times. The microchannels were then filled with M-CSF (20 ng ml^{-1}) containing RPMI medium. Then, 10 µl of macrophage suspension (4×10^7 cells per ml in medium) was added to the access ports and the cells were incubated for 45 min, before 3 ml medium was added on top. The microchannel dishes were then moved to an incubator and the macrophages were allowed to migrate into the microchannels for 18 h, before being imaged with a Zeiss LSM 780 confocal fluorescence microscope. For comparative analysis of macrophage invasion into the microchannels, the total signal of GFP-based cell volumes inside microchannels in each experiment was measured for control and knockout cells, and then displayed as a ratio of knockout to wild-type cells.

Electron microscopy

After removal of the brains, the tissue was fixed using 4% paraformaldehyde (Serva) and 1.5% glutaraldehyde (Serva) in PBS. Next, the tissue was dissected into blocks of approximately 1–2 mm^3 and stained with 0.5% osmium tetroxide (EMS) in PBS for 60 min. After rinsing in PBS and beginning dehydration in graded alcohol, the tissue was stained with 1% uranyl acetate (Merck) for one hour in 70% ethanol. Next, the tissue was further dehydrated in graded alcohol and finally propylene oxide (Sigma-Aldrich). The samples were transferred in Durcupan (Sigma-Aldrich), embedded in gelatin capsules and polymerized at 56 °C for 48 h. After polymerization, the blocks of resin were trimmed to prepare semi-thin sections using an ultra-microtome (Leica Microsystems) to identify regions of interest at the level of light microscopy. After finally trimming the blocks of resin, ultra-thin sections were prepared at a thickness of 55 nm, which were transferred on formvar-coated copper grids and stained with lead citrate. The analysis was performed using a Zeiss SIGMA electron microscope equipped with a STEM detector and ATLAS software (Zeiss NTS). Analyses included three mice for time point E14.5 and six mice for each time point of postnatal stages (P3, P10 and P21).

Immunohistochemistry

After transcardial perfusion with PBS, brains were fixed for 5 h in 4% PFA, dehydrated in 30% sucrose and embedded in Tissue-Tek OCT compound (Sakura Finetek). Cryosections were obtained as described previously[20]. Sections were cut at a thickness of 20 µm (only for the quantification of cell density), 30 µm or 50–60 µm (for quantification of the perivascular space (PVS) and for the analysis of $Mrc1^{CreERT2}R26^{Confetti}$ mice) and were then blocked with PBS containing 5% bovine serum albumin and permeabilized with 0.5% Triton-X100 in blocking solution. Primary antibodies were added overnight at a dilution of 1:1,000 for IBA1 (ab178846, Abcam; 234004, Synaptic Systems), 1:500 for CD206 (MCA2235, Biorad; AF2535, R&D systems), 1:200 for Col IV (AB769, Millipore), 1:1,000 for laminin (PA1-16730, Thermo Fisher Scientific), 1:500 for transferrin receptor (TfR; 8D3, Novus Biologicals), 1:200 for alpha smooth muscle actin (aSMA; 1A4, Thermo Fisher Scientific), 1:500 for NeuN (MAB377, Millipore), 1:500 for APC (OB80, Millipore), 1:500 for GFP (ab13970, Abcam), 1:500 for SOX9 (AF3075, R&D), 1:500 for P2Y12R (AS-55043A, Anaspec), 1:500 for Lyve1 (ALY7), Thermo Fisher Scientific), 1:500 for Ki-67 (ab15580, Abcam, SolA15, Thermo Fisher Scientific), 1:500 for cleaved active caspase 3 (559565, BD Biosciences), 1:500 for F4/80 (BM8, BioLegend), 1:1,000 for fibrinogen (F4203-02F, US Biological) or 1:200 for Cldn5 (352588, Invitrogen), at 4 °C. Secondary antibodies were purchased from Thermo Fisher Scientific or The Jackson Laboratory and added as follows: Alexa Fluor 405 1:1,000, Alexa Fluor 488 1:1,000, Alexa Fluor 568 1:1,000 and Alexa Fluor 647 1:1,000 for 2 h at room temperature. Coverslips were mounted with or without ProLong Diamond Antifade Mountant and with or without DAPI (Thermo Fisher Scientific). Human fetal brains were stained as follows: paraffin-embedded brain tissues were cut at 3 µm with a microtome. For deparaffinization, slides were initially incubated for 1 h at 80 °C followed by treatment with xylene. Rehydration was performed using a decreasing alcohol series. After cooking the slides in EnVision FLEX Target Retrieval Solution High pH cooking buffer for 40 min, the inactivation of the endogenous peroxidase was done by incubating with 3% hydrogen peroxidase for 10 min. Samples were blocked with 10% normal goat serum (NGS) plus 1% Triton X-100 in TRIS buffer. Incubation with the primary antibody (in 10% NGS, 1% Triton X-100 in TRIS buffer) was done at 4 °C overnight. After washing three times with TRIS buffer, a biotinylated secondary antibody (in 10% NGS, 1% Triton X-100 in TRIS buffer) was added and incubated for 45 min at room temperature. Samples were rinsed three times with TRIS buffer. Next, slides were incubated with DAB solution (1 drop EnVision Flex DAB Chromogen per 1 ml EnVision Flex Substrate Buffer). For double stainings, the procedure was repeated starting from the inactivation of the endogenous peroxidase. Streptavidin-AP and Permanent Red were used as conjugate and chromogen, respectively. Finally, the slides were counterstained with Gill's Hematoxylin. The following primary antibodies were used: CD206 (Abnova, H00004360-M02, 1:300), Col IV (GenomeMe, IHC549-100, 1:100) and P2ry12 (Sigma, HPA014518, 1:500). Biotinylated secondary antibodies were purchased from Southern Biotech and added at a dilution of 1:200.

Microscopy

Images were taken using a conventional fluorescence microscope (Olympus BX-61 with a colour camera (Olympus DP71) or BZ-9000 (Keyence) and the confocal pictures were taken with Fluoview FV1000 (Olympus, FV10-ASW v.4.2a software) using a 20× 1.0 NA (XLUMPlanFL N, Olympus) or with a TCS SP8 X (Leica, LAS X 3.5.7.23225) using a 20× 0.75 NA (HC PL APO 20×/0.75 IMM CORR CS2).

Cell quantification and quantification of the perivascular space

To assess the density of cells, numbers of IBA1$^+$CD206$^-$ (microglia) or CD206$^+$ cells (perivascular macrophages and meningeal macrophages) were quantified on a wide-field microscope (BZ-9000). Microglia and perivascular macrophages were normalized to the area of the region of interest and expressed as cells per mm^2. Meningeal macrophages were normalized to the length of the leptomeninges indicated by Col IV or laminin immunofluorescence and finally expressed as cells per mm. To assess the labelling efficacy for YFP, GFP or tdTomato, IBA1$^+$CD206$^-$ microglia, CD206$^+$ perivascular macrophages and meningeal macrophages, SOX9$^+$ astrocytes, NeuN$^+$ neurons and APC$^+$ oligodendrocytes were counted and analysed. At least three sections from a minimum of three mice were used for each analysis. Three-dimensionally reconstructed CD206$^+$ cell images and the sphericity score were obtained using Imaris software. For the quantification of clone sizes in Fig. 3h, i, 1.0-µm *z*-stacks were taken with a TCS SP8 X (Leica) confocal microscope. Different-coloured *confetti*$^+$ perivascular macrophages were distinguished on the basis of the cRFP signal or on the basis of the subcellular location of the anti-GFP signal (nGFP, nuclear; cYFP, cytosolic; mCFP, cell membrane). Clone sizes were determined by quantifying the same-coloured perivascular macrophages located at the same blood vessel. Five (P14) or ten (P28) sagittal sections were quantified. To measure the dimension of the PVS in Figs. 4a, b, 5f, 1.5 µm z-stacks were taken with a TCS SP8 X (Leica) confocal microscope. The maximum proximal PVS opening was measured directly below the pial surface and was defined as the widest distance between the inner Col IV$^+$ endothelial basement membrane and the outer laminin$^+$ basement membrane of the vessel. The proximal PVS was measured 50 µl below the pial surface and was defined as the difference between the diameter of the laminin$^+$ outer basement membrane and the vessel diameter.

Statistical analysis and data visualization

Statistical significance was determined using a Student's *t*-test or one-way ANOVA with post-hoc Tukey's multiple comparisons test using GraphPad Prism v.5.04 or v.9. Statistical testing and visualization of the next generation sequencing data was performed using specialized packages in the R programming environment[66].

Reporting summary

Further information on research design is available in the Nature Research Reporting Summary linked to this paper.

Data availability

The RNA-seq data that support the findings of this study have been deposited in the Gene Expression Omnibus (GEO) under accession codes GSE194432, GSE194433, GSE195437 and GSE192510. All other data that support the findings of this study are available from the corresponding authors upon reasonable request. Source data are provided with this paper.

Code availability

The code for the scRNA-seq analysis of yolk sac macrophage progenitors is available at https://github.com/rsankowski/Taka_A1_A2_only.

47. Sankowski, R., Monaco, G. & Prinz, M. Evaluating microglial phenotypes using single-cell technologies. *Trends Neurosci.* **45**, 133–144 (2022).
48. de Boer, J. et al. Transgenic mice with hematopoietic and lymphoid specific expression of Cre. *Eur. J. Immunol.* **33**, 314–325 (2003).
49. Petrich, B. G. et al. Talin is required for integrin-mediated platelet function in hemostasis and thrombosis. *J. Exp. Med.* **204**, 3103–3111 (2007).
50. Dono, R., Texido, G., Dussel, R., Ehmke, H. & Zeller, R. Impaired cerebral cortex development and blood pressure regulation in FGF-2-deficient mice. *EMBO J.* **17**, 4213–4225 (1998).
51. Mitchell, K. J. et al. Functional analysis of secreted and transmembrane proteins critical to mouse development. *Nat. Genet.* **28**, 241–249 (2001).
52. Potocnik, A. J., Brakebusch, C. & Fassler, R. Fetal and adult hematopoietic stem cells require β1 integrin function for colonizing fetal liver, spleen, and bone marrow. *Immunity* **12**, 653–663 (2000).
53. Feng, J. et al. IFN regulatory factor 8 restricts the size of the marginal zone and follicular B cell pools. *J. Immunol.* **186**, 1458–1466 (2011).
54. Snippert, H. J. et al. Intestinal crypt homeostasis results from neutral competition between symmetrically dividing Lgr5 stem cells. *Cell* **143**, 134–144 (2010).
55. Yu, W. M. et al. A Gata3-Mafb transcriptional network directs post-synaptic differentiation in synapses specialized for hearing. *eLife* **2**, e01341 (2013).
56. Hashimshony, T. et al. CEL-Seq2: sensitive highly-multiplexed single-cell RNA-seq. *Genome Biol.* **17**, 77 (2016).
57. Herman, J. S., Sagar, & Grun, D. FateID infers cell fate bias in multipotent progenitors from single-cell RNA-seq data. *Nat. Methods* **15**, 379–386 (2018).
58. Li, H. & Durbin, R. Fast and accurate long-read alignment with Burrows–Wheeler transform. *Bioinformatics* **26**, 589–595 (2010).
59. Baker, S. C. et al. The External RNA Controls Consortium: a progress report. *Nat. Methods* **2**, 731–734 (2005).
60. Grun, D., Kester, L. & van Oudenaarden, A. Validation of noise models for single-cell transcriptomics. *Nat. Methods* **11**, 637–640 (2014).
61. Picelli, S. et al. Full-length RNA-seq from single cells using Smart-seq2. *Nat. Protoc.* **9**, 171–181 (2014).
62. Dobin, A. et al. STAR: ultrafast universal RNA-seq aligner. *Bioinformatics* **29**, 15–21 (2013).
63. Harrow, J. et al. GENCODE: the reference human genome annotation for The ENCODE Project. *Genome Res.* **22**, 1760–1774 (2012).
64. Ritchie, M. E. et al. limma powers differential expression analyses for RNA-sequencing and microarray studies. *Nucleic Acids Res.* **43**, e47 (2015).
65. Paterson, N & Lämmermann, T. Macrophage network dynamics depend on haptokinesis for optimal local surveillance. *eLife* **11**, e75354 (2022).
66. R Core Team. *R: A Language and Environment for Statistical Computing* http://www.R-project.org/ (R Foundation for Statistical Computing, 2020).

Acknowledgements We thank E. Barleon and M. Fukuzaki for technical assistance and D. Grün and Sagar for their support with the preparation of the scRNA-seq data. We thank the Lighthouse Core Facility (LCF) for their support with cell sorting. LCF is funded in part by the Medical Faculty, University of Freiburg (Project numbers 2021/A2-Fol; 2021/B3-Fol) and the DFG (Project number 450392965). We are also grateful to R. Fässler and D. Critchley for providing mouse strains. T.M. was supported by AMED (JP20gm6310016 (PRIME), JP21wm0425001), JSPS (KAKENHI JP20K22687, JP21H02752, JP21H00204), the Kanae Foundation, the Naito Foundation, the Inamori Foundation and the Takeda Science Foundation. M.P. was supported by the Sobek Foundation, the Ernst Jung Foundation, the Novo Nordisk Prize, the DFG SFB 992 (Project ID 192904750), SFB1160 (Project ID 256073931), Reinhart-Koselleck-Grant (Project ID 279642606) and Gottfried Wilhelm Leibniz Prize, the Alzheimer Forschung Initiative e.V. (AFI) and the Ministry of Science, Research and Arts, Baden-Wuerttemberg (Sonderlinie 'Neuroinflammation'). This study was supported by the DFG under Germany's Excellence Strategy (CIBSS – EXC-2189 – Project ID 390939984). J.P. was supported by the UK DRI Momentum and Programme Leader Awards and the DFG SFB/TRR265. K.K. was supported by the Fritz Thyssen Foundation, by the DFG project grant (Project ID 432207796). K.K. and M.P. were supported by the DFG project grants within the CRC1479 (Project ID 441891347). K.K., K.-P.K., J.P., E.N., T.L. and M.P. were supported by the DFG-funded CRC/TRR167 'NeuroMac', Project ID 259373024. K.-P.K. was supported by the DFG GRK 2606 (Project ID 423813989). C.B. and U.L. were supported by the Swedish Brain Foundation and Erling-Persson Foundation. N.P. was supported by the DFG-funded project ID 89986987 (SFB 850).

Author contributions T.M. and L.A. designed experiments, analysed data and prepared the figures. G.M., R.S., O.S., M.K., F.D.G., L.H., M. Frosch, M. Fliegauf, A.Y. and L.F.P.B. performed experiments and analysed the data. E.N., N.P., F.F.-K., N.H., D.S., H.U., C.D., M.T., K.K., C.G., A.J., C.B., U.L., J.P., K.-P.K., R.D. and T.L. analysed the data and provided mice. J.P. and K.K. contributed to conception and critical revision. T.M. and M.P. supervised the project and wrote the manuscript.

Competing interests The authors declare no competing interests.

Additional information

Supplementary information The online version contains supplementary material available at https://doi.org/10.1038/s41586-022-04596-2.

Correspondence and requests for materials should be addressed to Takahiro Masuda or Marco Prinz.

Peer review information *Nature* thanks the anonymous reviewers for their contribution to the peer review of this work.

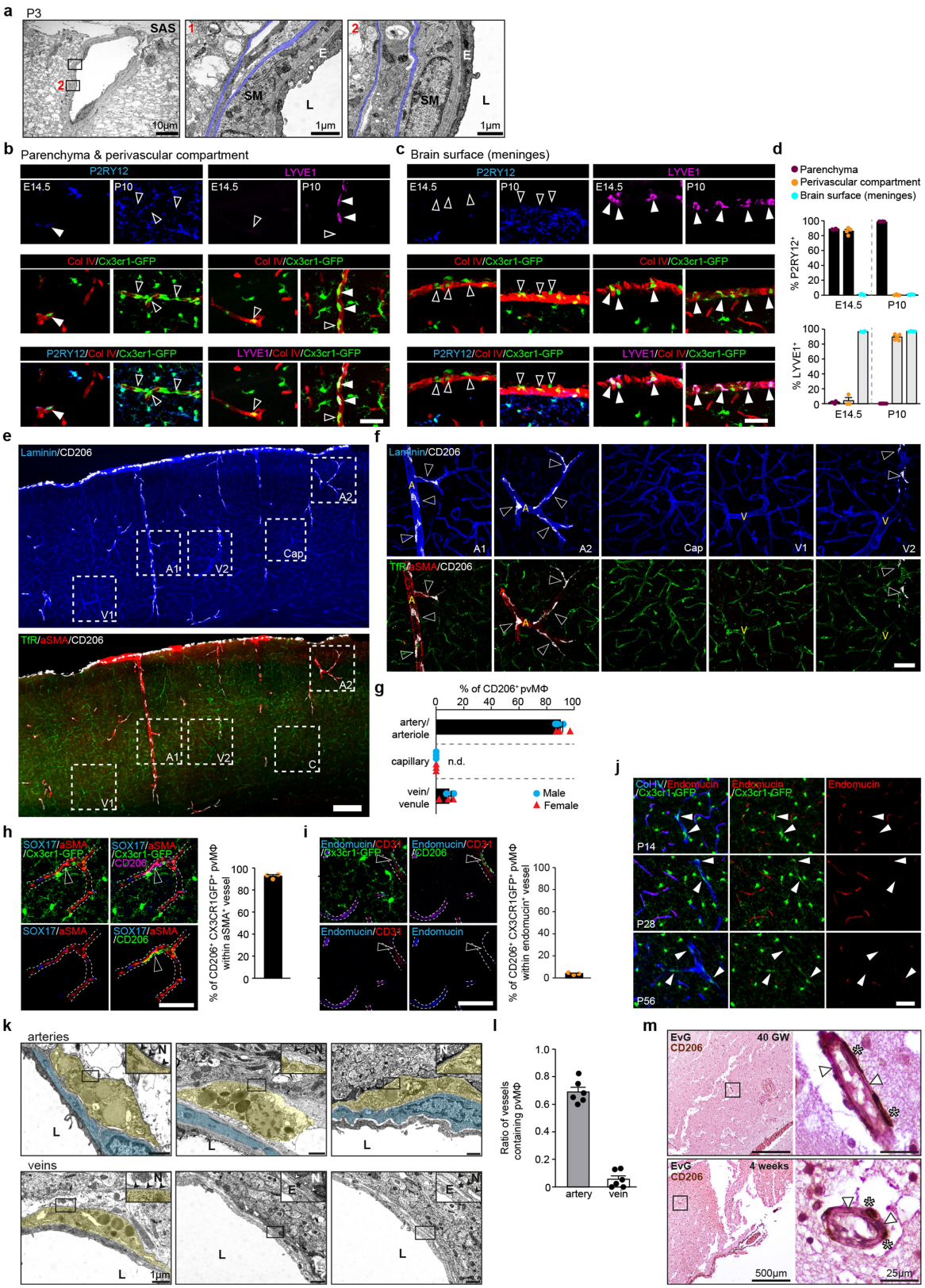

Extended Data Fig. 1 | See next page for caption.

Extended Data Fig. 1 | Preferential localization of perivascular macrophages in the arterial perivascular space during development in mice and humans. (**a**) Electron microscopy (EM) showing the establishment of a narrow PVS at P3 in the brains of wildtype mice. Blue: outer vascular and glial basal laminas. Representative images out of 6 mice investigated are shown. SAS: subarachnoid space; E: endothelium; SM: smooth muscle cell; L: vascular lumen. (**b**, **c**) P2RY12 (blue) and LYVE1 (magenta) and Col IV (red) immunofluorescence in the cortex of *Cx3cr1*$^{GFP/+}$ (green) mice. Arrowheads indicate double positive (filled) or single positive (blank) cells. Pictures representative out of at least three investigated mice per time point are shown. Scale bars: 50 µm. (**d**) Quantification thereof. Symbols represent individual mice. Bars indicate means ± s.e.m. (n = 4: E14.5 and P10 P2RY12, n = 3: E14.5 LYVE1, n = 5: P10 LYVE1). (**e**) Top: Immunofluorescence of CD206 (white) and laminin (blue, basement membranes) in the cortex of adult mice. Bottom: Most of the CD206$^+$ perivascular macrophages (pvMΦ) are located in alpha smooth muscle actin (aSMA, red)$^+$ transferrin receptor (TfR, green)$^-$ arteries/arterioles, with a minor population in aSMA$^-$TfR$^+$ veins/venules. Typical pictures out of 6 mice (3 male and 3 female) investigated are shown. A, artery/arteriole. Cap, capillary. V, vein/venule. Scale bar: 200 µm. (**f**) High-magnification images of dashed frames shown in **d**. Arrowheads indicate CD206$^+$ pvMΦ. Scale bar: 50 µm. (**g**) Distribution of CD206$^+$ pvMΦ in different vessels types (mean ± s.e.m., n = 3 mice for both genders). (**h**) Left: Immunofluorescence of CD206 (magenta or green), SOX17 (blue) and aSMA (red) in the cortex of adult *Cx3cr1*$^{GFP/+}$ (green) mice. Pictures representative of three mice investigated. Scale bar: 50 µm. Right: Frequency of CD206$^+$ CX3CR1–GFP$^+$ pvMΦ within aSMA$^+$ vessels (n = 3 mice). Three sections per mouse were quantified (means ± s.e.m.). (**i**) Left: Immunofluorescence of CD206 (green), endomucin (blue) CD31 (red) in the cortex of adult *Cx3cr1*$^{GFP/+}$ (green) mice. Pictures representative of three mice investigated. Scale bar. 50 µm. Right: quantification of CD206$^+$ CX3CR1–GFP$^+$ pvMΦ within endomucin$^-$ CD31$^+$ vessels (n = 3 mice). Three sections per mouse were quantified (means ± s.e.m.). (**j**) Representative images showing CX3CR1–GFP$^+$ pvMΦ in endomucin$^-$ Col IV$^+$ vessels at different developmental time points. Arrowheads indicate CX3CR1–GFP$^+$ pvMΦ located in the endomucin$^-$ vessels. Images representative of 3 mice for each timepoint investigated. Scale bar: 50 µm. (**k**) EM illustrating that pvMΦ (yellow) are preferentially localized in PVS of arterial vessels of wild-type mice at P21. Vascular smooth muscle cells (blue) are lacking in venous vessels. Images representative of 6 mice investigated. L: lumen, N: neuropil, E: endothelial cell. Arrows: glial basement membrane. Asterisks: processes of fibroblasts. (**l**) Distribution of pvMΦ around arteries and veins based on quantification in EM images in cortical sections of P21 mouse brains. Multiple non-consecutive sections per mouse were quantified. Symbols represent individual mice (n = 6, mean ± s.e.m.). (**m**) Immunohistochemistry for CD206 (brown) combined with Elastica-Van-Gieson (EvG) staining in human cortical brain. Asterisks: pvMΦ, arrowheads: EvG-positive arteries. Images representative of one sample per time point.

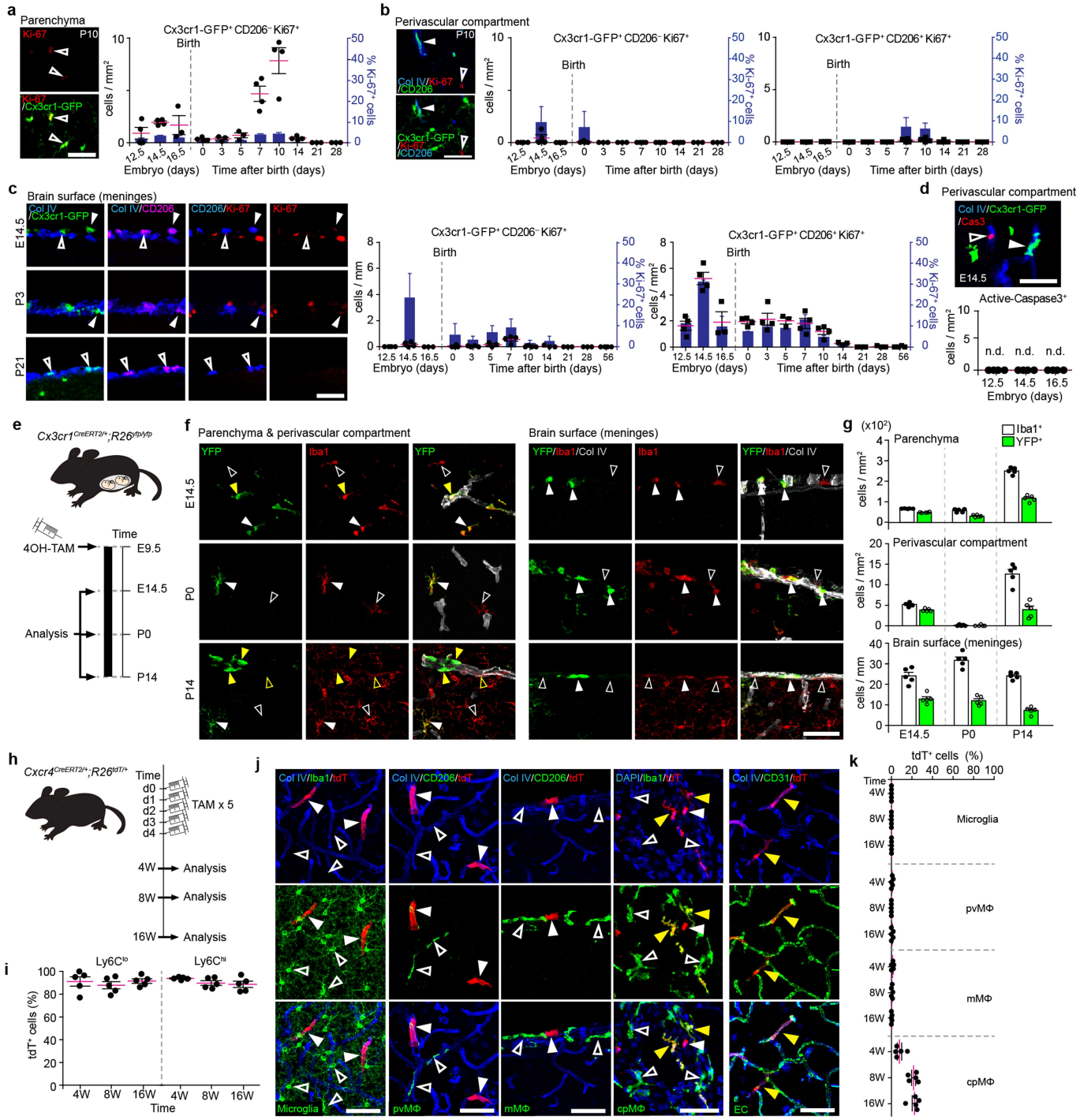

Extended Data Fig. 2 | See next page for caption.

Extended Data Fig. 2 | Kinetics of microglia, meningeal and perivascular macrophages as a HSC-independent cell population during development. (**a**) Left: representative images showing Ki-67$^+$ CX3CR1–GFP$^+$ cells in the parenchyma of *Cx3cr1*$^{GFP/+}$ mice at P10. Arrowheads indicate double positive cells. Representative pictures out of four mice investigated are shown. Scale bar. 50 µm. Right: density (cells / mm^2) and frequency (ratio of Ki-67$^+$ cells out of all CX3CR1–GFP$^+$ cells) of Ki-67$^+$ CD206$^-$ CX3CR1–GFP$^+$ cells in the parenchyma of *Cx3cr1*$^{GFP/+}$ mice during development (n=3 mice for E16.5, P3, P5, P21, P28; n = 4 mice for E12.5, E14.5, P0, P7, P10, P14). Three sections per mouse were quantified (means ± s.e.m.). (**b**) Left: representative images showing Ki-67$^+$ cells in the Col IV$^+$ perivascular compartment of *Cx3cr1*$^{GFP/+}$ mice at P10. Filled arrowheads: CD206$^+$ CX3CR1–GFP$^+$ Ki-67$^+$ cells, blank arrowheads: single Ki-67$^+$ cell. Images representative of four mice investigated. Scale bar: 50 µm. Right: density and frequency of Ki-67$^+$ CD206$^+$ CX3CR1–GFP$^+$ or Ki-67$^+$CD206$^-$CX3CR1–GFP$^+$ cells in the perivascular compartment of *Cx3cr1*$^{GFP/+}$ mice (n=3 mice for E16.5, P3, P5, P21, P28; n = 4 mice for E12.5, E14.5, P0, P7, P10, P14). Three sections/mouse were quantified (means ± s.e.m.). (**c**) Left, representative images showing Ki-67$^+$ or Ki-67$^-$ cells in the Col IV$^+$ brain surfaces of *Cx3cr1*$^{GFP/+}$ mice at E14.5, P3, and P21. Filled arrowhead indicate CD206$^+$CX3CR1–GFP$^+$Ki-67$^+$ cells, and blank arrowhead indicate CD206$^+$CX3CR1–GFP$^+$Ki-67$^-$ cells. Representative pictures out of four mice investigated are shown. Scale bar: 50 µm. Right, density and frequency of CD206$^+$CX3CR1–GFP$^+$Ki-67$^+$ or CD206$^-$ CX3CR1–GFP$^+$Ki-67$^+$ cells in the brain surfaces of *Cx3cr1*$^{GFP/+}$ mice during development (n=3 mice for E16.5, P5, P14, P21, P28; n = 4 mice for E12.5, E14.5, P0, P3, P7, P10, P56). Three sections per mouse were quantified (means ± s.e.m.). (**d**) Upper, representative images showing active-caspase 3 (Cas3)$^-$ CX3CR1–GFP (GFP)$^+$ cells in the perivascular compartment of *Cx3cr1*$^{GFP/+}$ mice at E14.5. Filled arrowhead indicates GFP$^+$Cas3$^-$ cell, and blank arrowhead indicates single Cas3$^+$ cell. Representative pictures out of four mice investigated are shown. Scale bar: 50 µm. Bottom, quantification of Cas3$^+$ CX3CR1–GFP$^+$ cells in the perivascular compartment of *Cx3cr1*$^{GFP/+}$ mice during embryogenesis (n = 4 for all timepoints). N.d., not detected. Three sections per mouse were quantified. (**e**) Scheme of experimental set-up. Pregnant *Cx3cr1*$^{CreERT2/+}$*R26*$^{YFP/YFP}$ females were injected with 4OH-TAM at E9.5, and the embryos or the offspring were then analysed at E14.5, P0, or P14, respectively. (**f**) Representative immunofluorescence images showing YFP-expressing IBA1$^+$ cells, in combination with Col IV$^+$ basal membrane, in the parenchyma, perivascular compartment, and brain surface of *Cx3cr1*$^{CreERT2/+}$*R26*$^{YFP/YFP}$ embryos (E14.5) or offspring (P0, P14). Filled yellow, filled white, blank white arrowheads indicate double positive cells in perivascular compartment, double positive cells in the parenchyma or meninges, or single positive cells, respectively. Representative pictures out of five mice investigated are shown. Scale bar: 50 µm. (**g**) Quantification thereof. Each symbol represents one mouse (n = 5). Means ± s.e.m. are shown. (**h**) Illustration of the experimental procedure for tamoxifen injection (TAM) and subsequent analysis of adult *Cxcr4*$^{CreERT2/+}$*R26*$^{tdT/+}$ mice. (**i**) Frequency of tdTomato (tdT)$^+$ Ly6C^{lo} and Ly6C^{hi} monocytes in the blood of *Cxcr4*$^{CreERT2/+}$*R26*$^{tdT/+}$ mice after tamoxifen injection (n = 5 mice for all timepoints tested). Data are depicted as mean ± s.e.m. (**j**) Typical images showing that tdT (filled white arrowheads) is not expressed in IBA1$^+$ microglia (green), CD206$^+$ pvMΦ (green) or CD206$^+$ meningeal macrophages (mMΦ, green), but in IBA1$^+$ choroid plexus macrophages (cpMΦ, green) and in the lumen of CD31$^+$ endothelial cells (green) in the brains of *Cxcr4*$^{CreERT2/+}$*R26*$^{tdT/+}$ mice 8 weeks after TAM injection. Yellow and blank arrowheads indicate double positive or single positive cells, respectively. EC, endothelial cell. Representative images out of 5 mice investigated are shown. Scale bars: 50 µm. (**k**) Frequency of tdT positive microglia, pvMΦ, and mMΦ in the cortex, and cpMΦ of *Cxcr4*$^{CreERT2/+}$*R26*$^{tdT/+}$ mice after TAM treatment (n = 5 mice for all timepoints tested). Data are depicted as mean ± s.e.m.

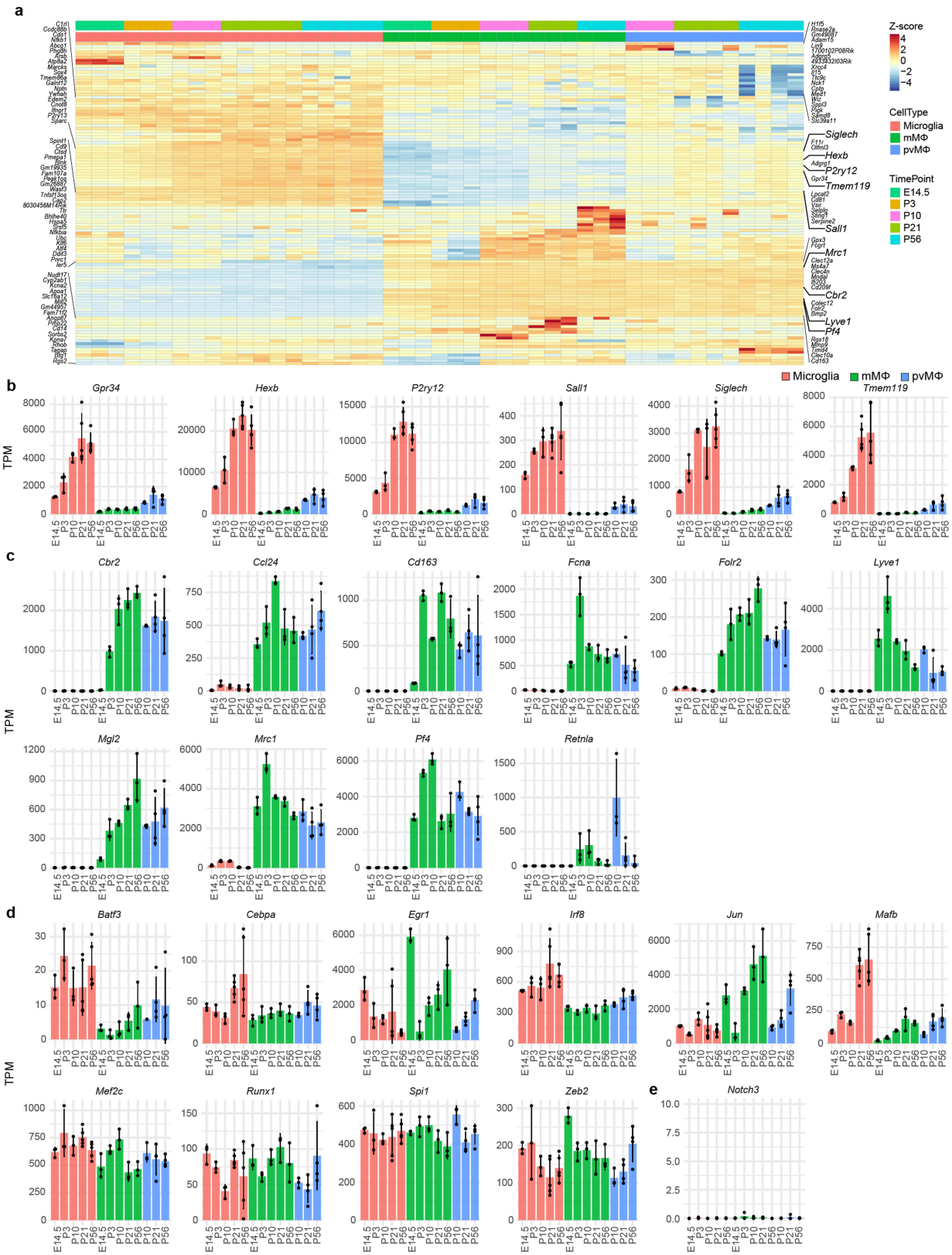

Extended Data Fig. 3 | Gene expression profiling reveals a stepwise development of microglia, meningeal and perivascular macrophages. (**a**) Heat map of the top 10 differentially regulated genes for each respective cell-type and time point. (**b**–**e**) Bar graphs depicting expression levels during development of microglia signature genes (**b**), CAM signature genes (**c**), transcription factors known to be expressed in macrophages (**d**) and *Notch3* (**e**). Means ± s.d. are shown. Each dot represents an individual sample. N= 3 for E14.5, P3 and P10 microglia, E14.5, P3, P10, P21 and P56 mMΦ, P10 pvMΦ; n = 4 for P21 and P56 pvMΦ; n = 5 for P21 and P56 microglia.

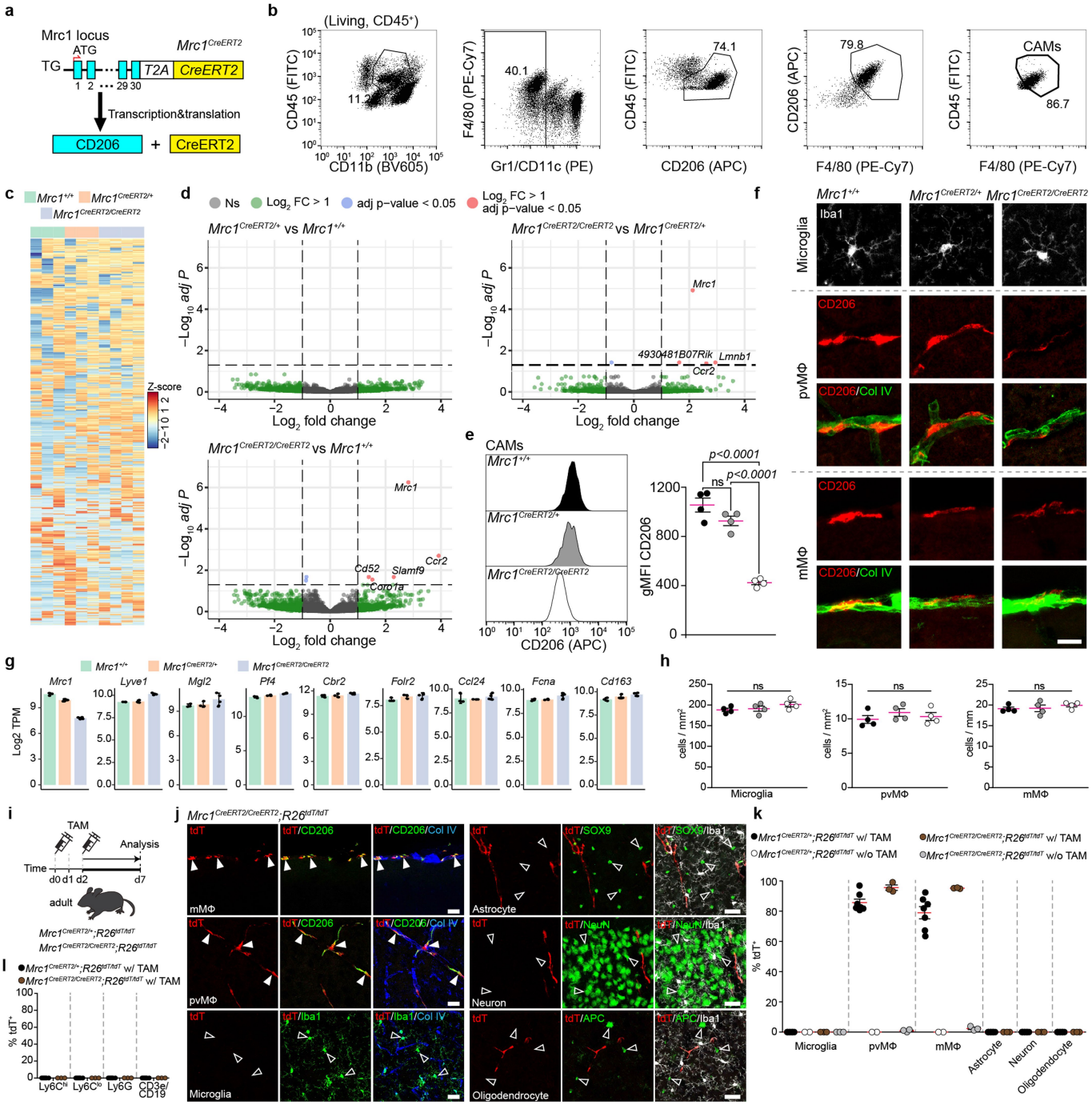

Extended Data Fig. 4 | See next page for caption.

Extended Data Fig. 4 | Generation and comparative analysis of *Mrc1*^{CreERT2} mice. (**a**) Targeting schemes. The T2A-CreERT2 cassette was knocked in into the *Mrc1* locus just before the stop codon. From the resulting polycistronic RNA, a fusion protein is translated, which gives rise to MRC1 (CD206) and the CreERT protein through the activity of the self-cleaving T2A peptide. (**b**) Representative gating strategy for FACS-sorting of CD206$^+$ CAMs from adult *Mrc1*$^{+/+}$, *Mrc1*$^{CreERT2/+}$ or *Mrc1*$^{CreERT2/CreERT2}$ mice for RNA-expression analysis and for measuring CD206 surface expression levels. (**c**) Heat map of the top 1,000 differentially regulated genes across the respective genotypes. (**d**) Volcano plots depicting differentially regulated genes between the groups (14,639 variables) (n = 3 for *Mrc1*$^{+/+}$ and *Mrc1*$^{CreERT2/+}$, n = 4 for *Mrc1*$^{CreERT2/CreERT2}$). NS = not significant. (**e**) Left: Representative histograms showing CD206 surface expression levels on CAMs isolated using the gating strategy depicted in (**b**). Right: Quantification geometric mean fluorescence intensities (gMFI). Symbols represent individual mice (means ± s.e.m. are shown). N = 4 mice per genotype. One-way ANOVA with Tukey's multiple comparisons test. (**f**) Immunofluorescence images showing IBA1$^+$ (white) microglia, CD206$^+$ (red) pvMΦ and CD206$^+$ mMΦ in the cortex of *Mrc1*$^{+/+}$, *Mrc1*$^{CreERT2/+}$ or *Mrc1*$^{CreERT2/CreERT2}$ mice. Images representative of 4 mice per genotype. Scale bar: 20 µm (**g**) Bar graphs depicting the expression levels of CAM signature genes. Dots represent individual mice (mean ± s.d.). (n = 3 for *Mrc1*$^{+/+}$ and *Mrc1*$^{CreERT2/+}$, n = 4 for *Mrc1*$^{CreERT2/CreERT2}$). (**h**) Quantification of microglia, pvMΦ and mMΦ in the cortex of adult *Mrc1*$^{+/+}$ (black circles), *Mrc1*$^{CreERT2/+}$ (grey circles) or *Mrc1*$^{CreERT2/CreERT2}$ (white circles) mice. Each symbol represents one mouse (n = 4 for all genotypes). Three sections per mouse were quantified (means ± s.e.m.). One-way ANOVA with Tukey's multiple comparisons test. (**i**) Scheme of the experimental set-up. (**j**) Direct fluorescence microscopic visualization reveals tdT signals (red) in CD206$^+$ pvMΦ and mMΦ (green), but not in microglia (IBA1, green), astrocytes (SOX9, green), neurons (NeuN, green), or oligodendrocyte (APC, green) in the cortex of adult *Mrc1*$^{CreERT2/CreERT2}$*R26*$^{tdT/tdT}$ mice. Col IV is shown in blue. Filled arrowheads indicate double positive pvMΦ and mMΦ, empty triangles show single positive cells. Images representative of three mice. Scale bars: 20 µm. (**k**) Quantification of recombination efficacy in several CNS cells of *Mrc1*$^{CreERT2/CreERT2}$*R26*$^{tdT/tdT}$ and *Mrc1*$^{CreERT2/+}$*R26*$^{tdT/tdT}$ mice (with or without TAM), respectively. Each symbol represents one mouse (*Mrc1*$^{CreERT2/+}$*R26*$^{tdT/tdT}$ with TAM, n = 7; *Mrc1*$^{CreERT2/+}$*R26*$^{tdT/tdT}$ without TAM, n = 2; *Mrc1*$^{CreERT2/CreERT2}$*R26*$^{tdT/tdT}$ with TAM, n = 3; *Mrc1*$^{CreERT2/CreERT2}$*R26*$^{tdT/tdT}$ without TAM, n = 3). Three sections per mouse were quantified (means ± s.e.m.). (**l**) Flow cytometry-based quantification of tdT-labelled blood immune cells. Each symbol represents one mouse (*Mrc1*$^{CreERT2/+}$*R26*$^{tdT/tdT}$, n = 6; *Mrc1*$^{CreERT2/CreERT2}$*R26*$^{tdT/tdT}$, n = 3. Data are shown as mean ± s.e.m.

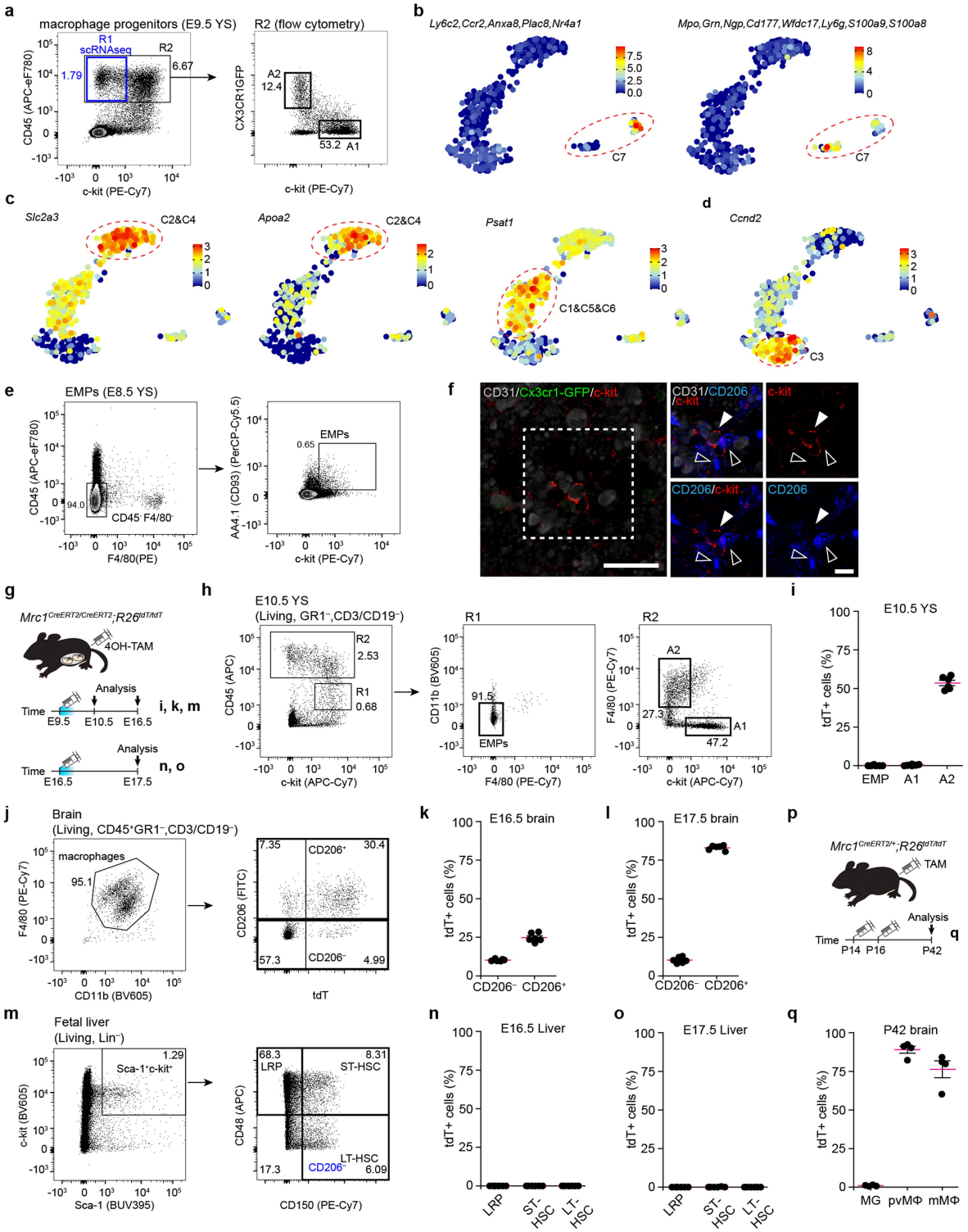

Extended Data Fig. 5 | See next page for caption.

Extended Data Fig. 5 | An *Mrc1*$^{+}$ A2 population in the yolk sac gives rise to both microglia and CAMs. (**a**) Gating strategies for yolk sac macrophage progenitors. c-Kit^{lo}CD45^{+} cells (R1, blue) isolated from the wild-type yolk sac at E9.5 were used for scRNA-seq shown in Fig. 3a–d. CX3CR1–GFP^{-}c-Kit^{+} A1 and CX3CR1–GFP^{+}c-Kit^{-} A2 cells isolated from the yolk sac of *Cx3cr1*$^{GFP/+}$ mice were used for the analysis shown in Fig. 3e, **f**. Representative plots out of three mice are shown. (**b**) UMAP plots representing the core signature genes for monocytes (left) and granulocytes (right) in the yolk sac. (**c**) UMAP plots of genes that are enriched in clusters C2 and C4 (*Slc2a3* and *Apoa2*), or C1, C5 and C6 (*Psat1*) are shown (483 yolk sac cells). Each dot represents a single cell. (**d**) UMAP plot of *Ccnd2* gene enriched in cluster C3 is shown (483 yolk sac cells). Each dot represents a single cell. (**e**) Gating strategies for EMPs are shown. c-Kit^{+}AA4.1^{+}CD45$^{neg\text{-}lo}$F4/80^{-} cells isolated from the *Cx3cr1*$^{GFP/+}$ yolk sac at E8.5 were used for the analysis shown in Fig. 3e, **f**. Representative plots out of four mice are shown. (**f**) Representative immunofluorescence images depicting CD206^{-} c-Kit^{+} EMPs in the yolk sac at E8.5 of *Cx3cr1*$^{GFP/+}$ pregnant females. Immunolabelling was performed for c-Kit (red), CD206 (blue) and CD31 for yolk sac endothelia cells (white), respectively. White filled arrowhead indicates CD206^{-} c-Kit^{+} EMPs, and blank white arrowheads indicate CD206^{+} yolk sac cells. Representative pictures out of four yolk sac investigated are shown. Scale bars: 50 µm, 20 µm (inset). (**g**) Scheme of the experimental set-up. (**h**) Representative gating strategy for EMPs, A1 and A2 cells isolated from the yolk sac of *Mrc1*$^{CreERT2/CreERT2}$*R26*$^{tdT/tdT}$ embryos at E10.5. Plots show six individual yolk sacs that were concatenated for representation. (**i**) Quantification of tdT-expressing EMPs, A1 and A2 cells isolated from the yolk sac of *Mrc1*$^{CreERT2/CreERT2}$*R26*$^{tdT/tdT}$ embryos at E10.5 (n = 6). (**j**–**l**) Representative gating strategy (**j**) for the quantification of tdT-expressing CD206^{-} and CD206^{+} macrophages isolated from the brains of *Mrc1*$^{CreERT2/CreERT2}$*R26*$^{tdT/tdT}$ embryos at E16.5 (**k**: n = 6) or E17.5 (**l**: n = 6). (**m**–**o**) Representative gating strategy (**m**) for the quantification of tdT-expressing lineage-restricted progenitors (LRP), short-term (LT-) hematopoietic stem cells (HSC) and long-term (LT-) HSC isolated from the fetal livers of *Mrc1*$^{CreERT2/CreERT2}$*R26*$^{tdT/tdT}$ embryos at E16.5 (**n**: n = 6) or E17.5 (**o**: n = 6). (**p**) Scheme of the experimental set-up. (**q**) Quantification of tdT^{+} microglia, pvMΦ and mMΦ in *Mrc1*$^{CreERT2/+}$*R26*$^{tdT/tdT}$ mice. Each symbol represents one mouse (n = 4 mice). Three sections/mouse were quantified (means ± s.e.m.).

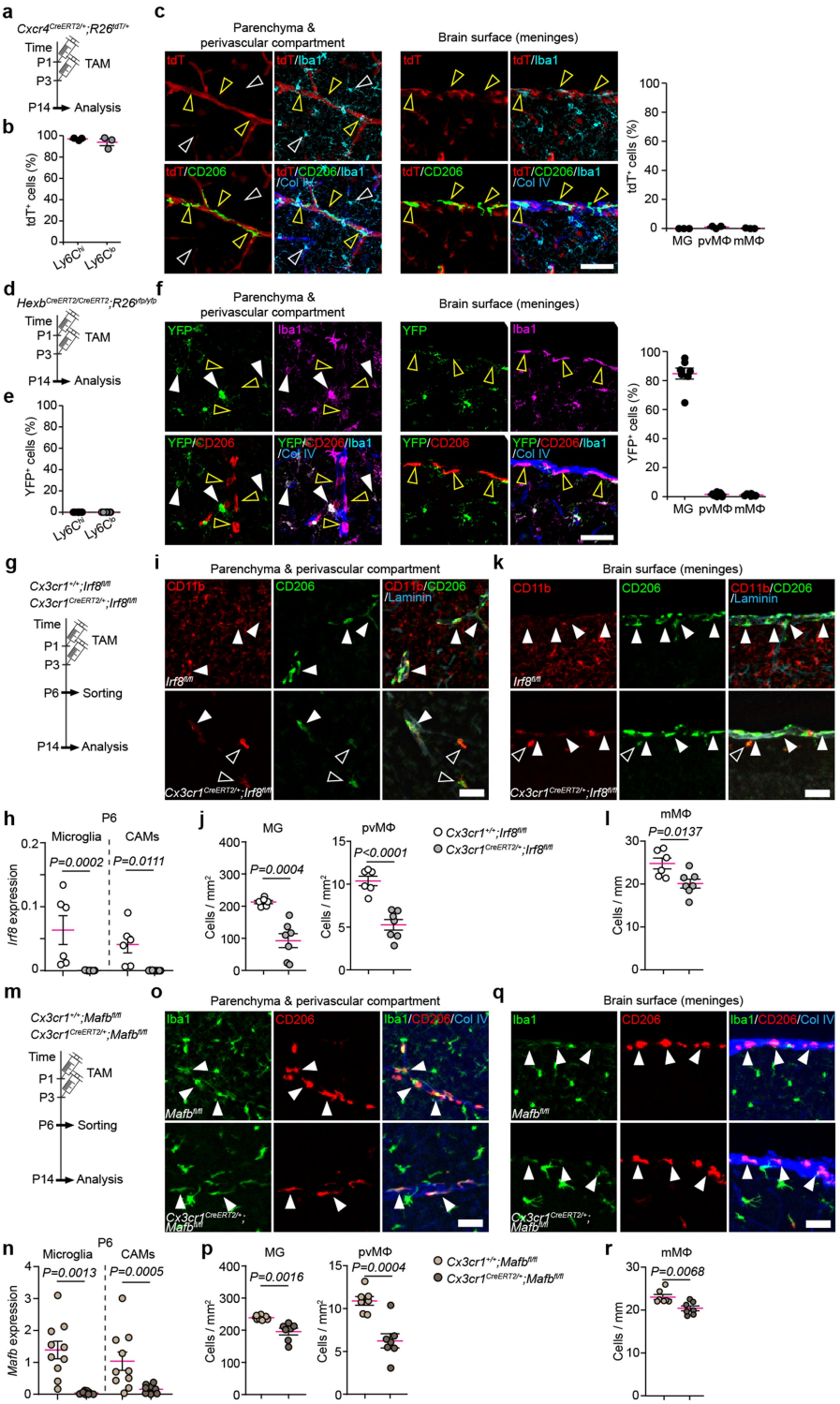

Extended Data Fig. 6 | See next page for caption.

Extended Data Fig. 6 | No contribution of bone-marrow-derived cells or microglia to the pool of perivascular macrophages during development, but dependence on the transcription factors *Irf8* and *Mafb*. (**a**) Scheme of the experimental set-up. (**b**) Flow cytometry-based quantification of tdT-labelled Ly6C^{hi} or Ly6c^{lo} blood monocytes in *Cxcr4*$^{CreERT2/+}$*R26*$^{tdT/+}$ mice (n = 3). Symbols represent individual mice. Data are shown as mean ± s.e.m. (**c**) Left, representative immunofluorescence images of tdT signals (red) in vessel cells, but not in pvMΦ (CD206, green) and microglia (IBA1, cyan), combined with immunofluorescence for Col IV (blue), from *Cxcr4*$^{CreERT2/+}$*R26*$^{tdT/tdT}$ mice at P14. Blank white, and blank yellow arrowheads indicate single positive microglia or single positive pvMΦ, respectively. Representative images from three mice are depicted. Scale bars: 50 µm. Right, quantification of tdT-expressing microglia (MG, IBA1), pvMΦ (CD206) and mMΦ (CD206) in *Cxcr4*$^{CreERT2/+}$*R26*$^{tdT/tdT}$ mice. Each symbol represents one mouse (n = 3). Three sections per mouse were quantified (means ± s.e.m.). (**d**) Scheme of experimental set-up. (**e**) Flow cytometry-based quantification of YFP-labelled Ly6C^{hi} or Ly6c^{lo} blood monocytes in *Hexb*$^{CreERT2/CreERT2}$*R26*$^{YFP/YFP}$ mice (n = 7). Each symbol represents one mouse. Data are shown as mean ± s.e.m. (**f**) Left, representative immunofluorescence images of YFP signals (green) in microglia (IBA1, purple), but not in pvMΦ (CD206, red) and mMΦ (CD206, red), combined with immunofluorescence for Col IV (blue), from *Hexb*$^{CreERT2/CreERT2}$*R26*$^{YFP/YFP}$ mice at P14. Filled white and blank yellow arrowheads indicate double positive microglia or single positive pvMΦ/mMΦ, respectively. Representative images from seven mice are depicted. Scale bars: 50 µm. Right, quantification of YFP-expressing microglia (MG, IBA1^{+}), pvMΦ (CD206^{+}) and mMΦ (CD206^{+}) in *Hexb*$^{CreERT2/CreERT2}$*R26*$^{YFP/YFP}$ mice. Each symbol represents one mouse (n = 7). Three sections per mouse were quantified. Means ± s.e.m. (**g**) Scheme of experimental set-up. (**h**) Quantitative PCR of *Irf8* mRNA levels in sorted microglia and CAMs from *Cx3cr1*$^{CreERT2/+}$*Irf8*$^{fl/fl}$ and controls at P6. Each symbol represents one mouse (n = 6 for control, n = 10 for *Cx3cr1*$^{CreERT2/+}$*Irf8*$^{fl/fl}$). Two-sided unpaired *t*-test. (**i**) Representative immunofluorescence images from the cortex of *Cx3cr1*$^{CreERT2/+}$*Irf8*$^{fl/fl}$ and control mice for CD11b (red), CD206 (green) and laminin (blue) depicting microglia (blank arrowheads) and pvMΦ (filled arrowheads). Scale bars: 50 µm. (**j**) Quantification of microglia (MG) and pvMΦ. Each symbol represents one mouse (*Irf8*$^{fl/fl}$, n = 6; *Cx3cr1*$^{CreERT2/+}$*Irf8*$^{fl/fl}$, n = 7). Three sections per mouse were quantified. Means ± s.e.m. Two-sided unpaired *t*-test. (**k**) Histological pictures from the meninges of *Cx3cr1*$^{CreERT2/+}$*Irf8*$^{fl/fl}$ and control mice for CD11b (red), CD206 (green) and laminin (blue) showing microglia (blank arrowheads) and mMΦ (filled arrowheads). Scale bars: 50 µm. (**l**) Quantification thereof. Each symbol represents one mouse (*Irf8*$^{fl/fl}$, n = 6; *Cx3cr1*$^{CreERT2/+}$*Irf8*$^{fl/fl}$, n = 7). Three sections per mouse were quantified. Means ± s.e.m. Two-sided unpaired *t*-test. (**m**) Scheme of experimental set-up. (**n**) Quantitative PCR of *Mafb* mRNA levels in sorted microglia and CAMs from *Cx3cr1*$^{CreERT2/+}$*Mafb*$^{fl/fl}$ (n = 9 mice) and controls (n = 10 mice) at P6. Each symbol represents one mouse. Two-sided unpaired *t*-test. (**o**) Typical histological images from the cortex of *Cx3cr1*$^{CreERT2/+}$*Mafb*$^{fl/fl}$ and control mice for CD11b (red), CD206 (green) and laminin (blue) depicting pvMΦ (filled arrowheads). Scale bars: 50 µm. (**p**) Quantification of microglia (MG) and pvMΦ. Each symbol represents one mouse (n = 7 per genotype). Three sections per mouse were quantified. Means ± s.e.m. Two-sided unpaired *t*-test. (**q**) Histological pictures from the meninges of *Cx3cr1*$^{CreERT2/+}$*Mafb*$^{fl/fl}$ mice for CD11b (red), CD206 (green) and laminin (blue) showing mMΦ (filled arrowheads). Scale bars: 50 µm. (**r**) Quantification thereof. Each symbol represents one mouse (n = 7 per genotype). Three sections per mouse were examined. Means ± s.e.m. Two-sided unpaired *t*-test.

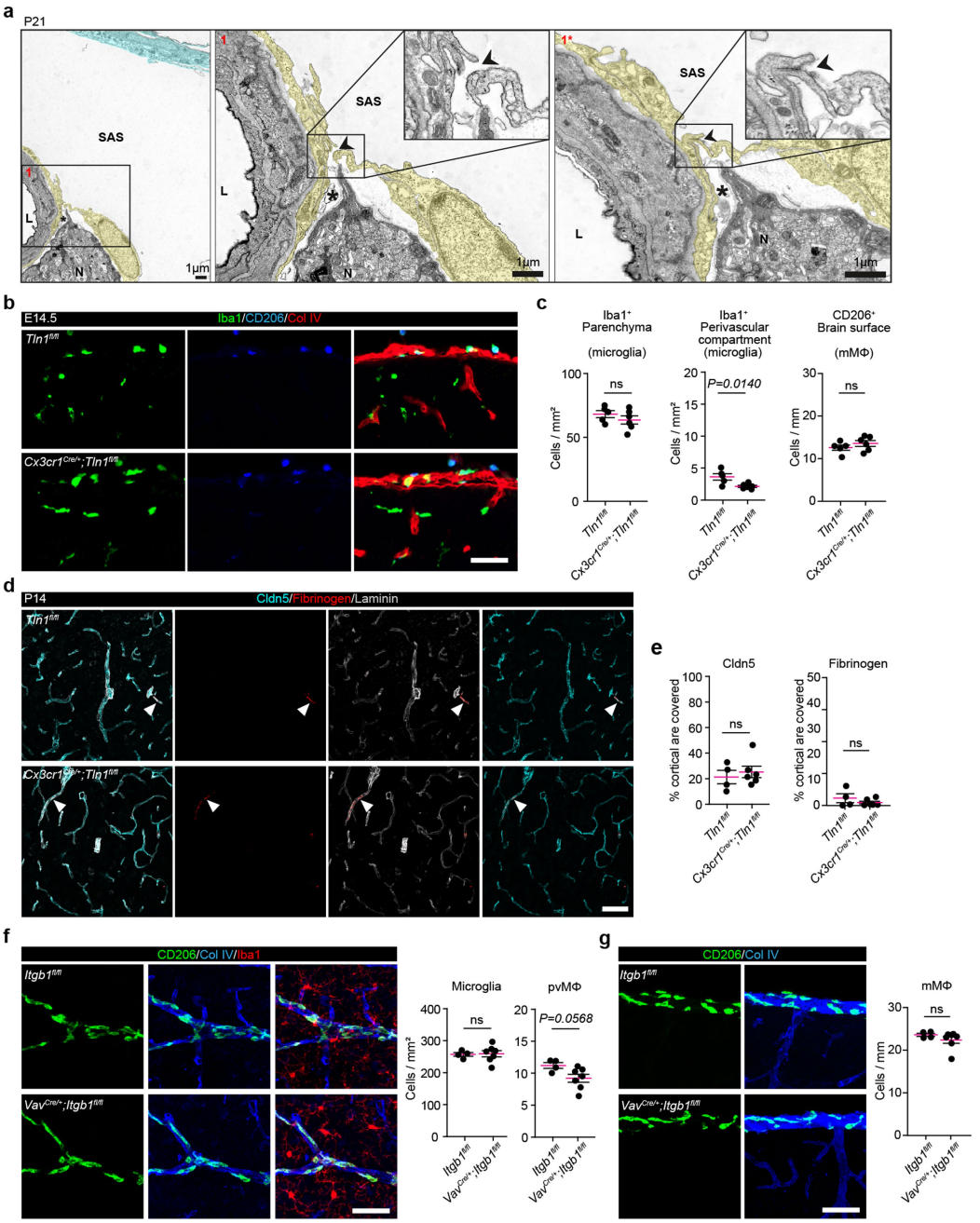

Extended Data Fig. 7 | Different roles of integrin signalling in the development of microglia, meningeal and perivascular macrophages. (**a**) Illustrative electron microscopy images depicting the intersection of a brain-penetrating arterial blood vessel with the leptomeninges. Left: overview, 1: higher magnification of the area indicated in the overview image and a consecutive section (1*) of the same area. Arrowheads depicting a gap (in 1) and a direct contact (in 1*) between processes of pial cells that cover the PVS. Yellow: pia mater, Blue: arachnoid mater, Asterisk: PVS, L: vessel lumen, N: neuropil. Representative images out of 6 mice investigated are shown. (**b**) Representative images showing IBA1$^+$ or CD206$^+$ cells in the parenchyma, the perivascular compartment, or the brain surface of either control *Tln*$^{fl/fl}$ or *Cx3cr1*^{Cre}*Tln*$^{fl/fl}$ embryos at E14.5. Col IV staining (red) was also included. Representative images from five (*Tln*$^{fl/fl}$) or six mice (*Cx3cr1*^{Cre}*Tln*$^{fl/fl}$) are depicted. Scale bars: 50 µm. (**c**) Quantification thereof. Each symbol represents one embryo (n = 5 for *Tln*$^{fl/fl}$; n = 6 for *Cx3cr1*^{Cre}*Tln*$^{fl/fl}$). Three sections/mouse were quantified (means ± s.e.m.). Two-sided unpaired *t*-test. Ns: not significant. (**d**) Representative images showing claudin 5 (Cldn5, cyan), fibrinogen (red) and laminin (grey) immunoreactivity in the cortex of *Cx3cr1*$^{Cre/+}$*Tln1*$^{fl/fl}$ and *Tln1*$^{fl/fl}$ controls. Arrowheads indicate fibrinogen immunofluorescence within the vessel lumen. Representative images from four (*Tln*$^{fl/fl}$) or six mice (*Cx3cr1*^{Cre}*Tln*$^{fl/fl}$) are depicted. Scale bar: 50 µm. (**e**) Quantification of the area covered by Cldn5 or fibrinogen immunofluorescence, respectively. Each symbol represents one mouse (n = 4 for *Tln*$^{fl/fl}$; n = 6 for *Cx3cr1*^{Cre}*Tln*$^{fl/fl}$). Three sections per mouse were quantified (means ± s.e.m.). Two-sided unpaired *t*-test. Ns: not significant. (**f**) Left, representative immunofluorescence images of IBA1$^+$ microglia (red) and CD206$^+$ pvMΦ (green), combined with immunofluorescence for Col IV (blue), in control *Itgb1*$^{fl/fl}$ and *Vav*^{Cre}*Itgb1*$^{fl/fl}$ mice at P14. Representative images from four (*Itgb1*$^{fl/fl}$) or seven (*Vav*^{Cre}*Itgb1*$^{fl/fl}$) mice are depicted. Scale bar: 50 µm. Right, quantification thereof (n = 4 for *Itgb1*$^{fl/fl}$, n = 7 for *Vav*^{Cre}*Itgb1*$^{fl/fl}$). Three sections per mouse were quantified (means ± s.e.m.). Two-sided unpaired *t*-test. (**g**) Left, representative immunofluorescence images of CD206$^+$ mMΦ green) with Col IV$^+$ basement membranes (blue) in control *Itgb1*$^{fl/fl}$ and *Vav*^{Cre} *Itgb1*$^{fl/fl}$ mice at P14. Representative images from four (*Itgb1*$^{fl/fl}$) or seven (*Vav*^{Cre}*Itgb1*$^{fl/fl}$) mice are depicted. Scale bar: 50 µm. Right, quantification thereof (n = 4 for *Itgb1*$^{fl/fl}$, n = 7 for *Vav*^{Cre}*Itgb1*$^{fl/fl}$). Three sections per mouse were quantified (means ± s.e.m.). Two-sided unpaired *t*-test.

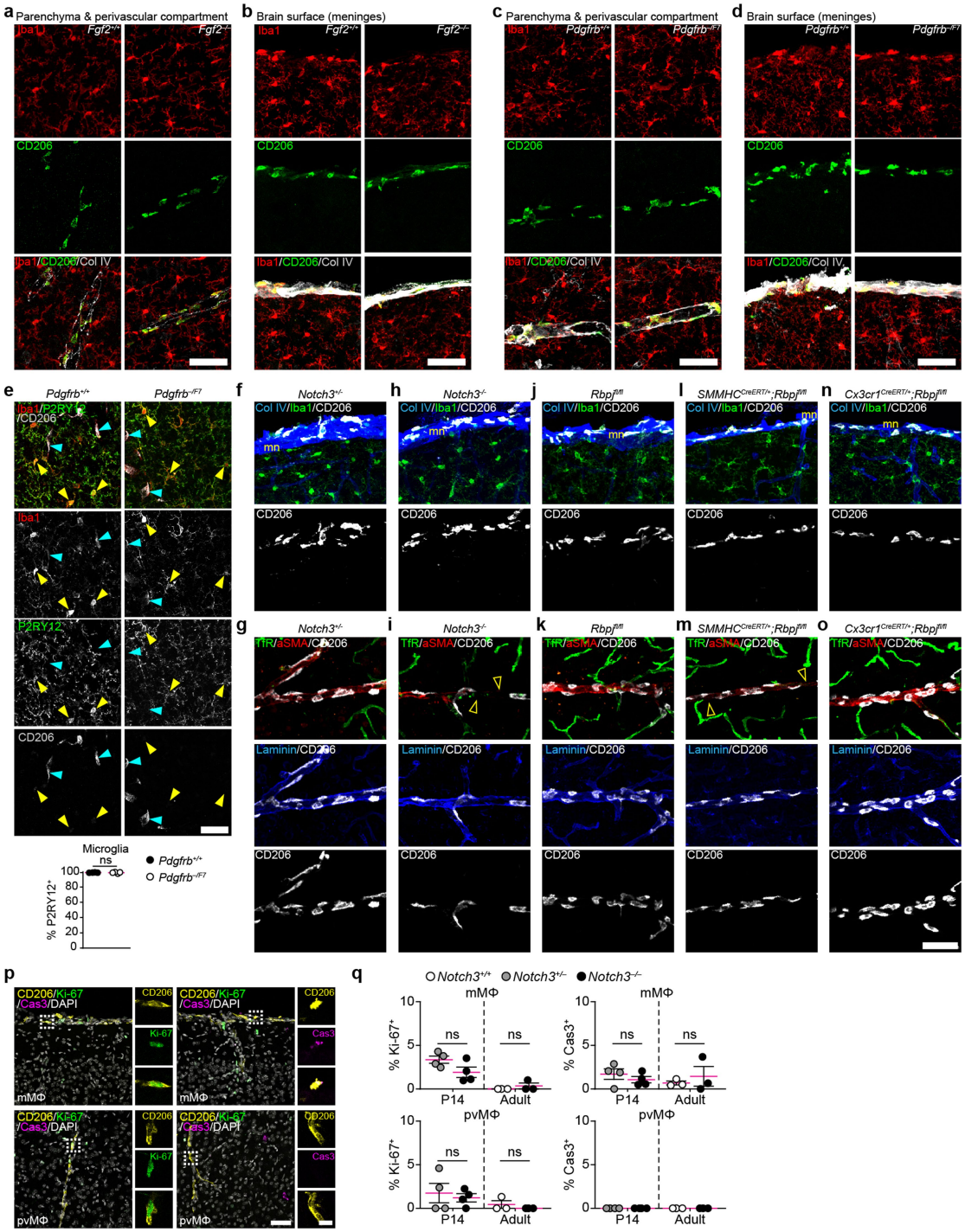

Extended Data Fig. 8 | See next page for caption.

Extended Data Fig. 8 | Distribution of microglia, meningeal and perivascular macrophages in the brains of *Fgf2*$^{-/-}$ or *Pdgfrb*$^{-/F7}$ mice. (**a**, **b**) Representative immunofluorescence of IBA1^{+} microglia (red), CD206^{+} pvMΦ (green) and Col IV^{+} basement membranes (white) in the cortex of *Fgf2*$^{+/+}$ or *Fgf2*$^{-/-}$ mice (**a**), and *Pdgfrb*$^{+/+}$ or *Pdgfrb*$^{-/F7}$ mice (**c**) at P14. Images representative of 3 (*Fgf2*$^{+/+}$ or *Fgf2*$^{-/-}$), 4 (*Pdgfrb*$^{+/+}$) or 5 (*Pdgfrb*$^{-/F7}$) mice. Scale bar: 30µm. (**b**, **d**) Representative immunofluorescence of IBA1^{+} (red) CD206^{+} (green) mMΦ and Col IV^{+} meninges (white) in the cortical surfaces of *Fgf2*$^{+/+}$ or *Fgf2*$^{-/-}$ mice (**b**), and *Pdgfrb*$^{+/+}$ or *Pdgfrb*$^{-/F7}$ mice (**d**) at P14. Images representative of 3 (*Fgf2*$^{+/+}$ or *Fgf2*$^{-/-}$), 4 (*Pdgfrb*$^{+/+}$) or 5 (*Pdgfrb*$^{-/F7}$) mice. Scale bar: 30 µm. (**e**) Upper: Representative images from the cortex of *Pdgfrb*$^{+/+}$ or *Pdgfrb*$^{-/F7}$ mice at P14. Yellow arrowheads depict IBA1^{+} (red) P2ry12^{+} (green) CD206^{-} (grey) microglia and cyan arrowheads reveal IBA1^{+} P2ry12^{-} CD206^{+} pvMΦ. Images are representative of four mice per genotype. Lower: The amount of P2ry12^{+} microglia was quantified. Symbols represent individual moice (n = 4 for both genotypes). Three sections per mouse were quantified (means ± s.e.m.). Two-sided unpaired *t*-test. Ns: not significant. (**f**, **h**, **j**, **l**, **n**) Immunofluorescence of microglia (IBA1, green) and mMΦ (CD206, white), in combination with Col IV^{+} basal membrane (blue), in *Notch3*$^{+/-}$ (**f**), *Notch3*$^{-/-}$ (**h**), *Rbpj*$^{fl/fl}$ (**j**), *SMMHC*^{CreERT2}*Rbpj*$^{fl/fl}$ (**l**), and *Cx3cr1*$^{CreERT2/+}$*Rbpj*$^{fl/fl}$ mice (**n**), respectively. Representative images from 8 (*Notch3*$^{+/-}$, *Notch3*$^{-/-}$), 6 (*Rbpj*$^{fl/fl}$), 7 (*SMMHC*^{CreERT2}*Rbpj*$^{fl/fl}$), and 4 (*Cx3cr1*$^{CreERT2/+}$*Rbpj*$^{fl/fl}$) mice are depicted. Scale bar: 50 µm. (**g**, **i**, **k**, **m**, **o**) Immunofluorescence of pvMΦ (CD206, white) in the aSMA^{+}(red) TfR^{-}(green) artery in combination with laminin for basement membranes (blue) in *Notch3*$^{+/-}$ (**g**), *Notch3*$^{-/-}$ (**i**), *Rbpj*$^{fl/fl}$ (**k**), *SMMHC*^{CreERT2}*Rbpj*$^{fl/fl}$ (**m**), and *Cx3cr1*$^{CreERT2/+}$*Rbpj*$^{fl/fl}$ mice (**o**), respectively. Representative images from 8 (*Notch3*$^{+/-}$, *Notch3*$^{-/-}$), 6 (*Rbpj*$^{fl/fl}$), 7 (*SMMHC*^{CreERT2}*Rbpj*$^{fl/fl}$), and 4 (*Cx3cr1*$^{CreERT2/+}$*Rbpj*$^{fl/fl}$) mice are shown. Scale bar: 50 µm. (**p**) Representative images of Ki-67 (green) and cleaved-caspase3 (Cas3, magenta) immunoreactivity in CD206^{+} (white) mMΦ (top) or CD206^{+} pvMΦ (bottom) in *Notch3*$^{+/-}$ and *Notch3*$^{-/-}$ mice at P14 (n = 4). Scale bars: 50 µm, 10 µm (insets). (**q**) Quantification of Ki-67^{+} or Cas3^{+} mMΦ (top) and pvMΦ (bottom) in the cortex of *Notch3*$^{+/+}$ (adult: n = 3), *Notch3*$^{+/-}$ (P14: n = 4) and *Notch3*$^{-/-}$ (P14: n = 4, adult: n = 3) mice at indicated time points. Three sections per mouse were quantified (means ± s.e.m.). Each symbol represents one mouse. Ns: not significant.

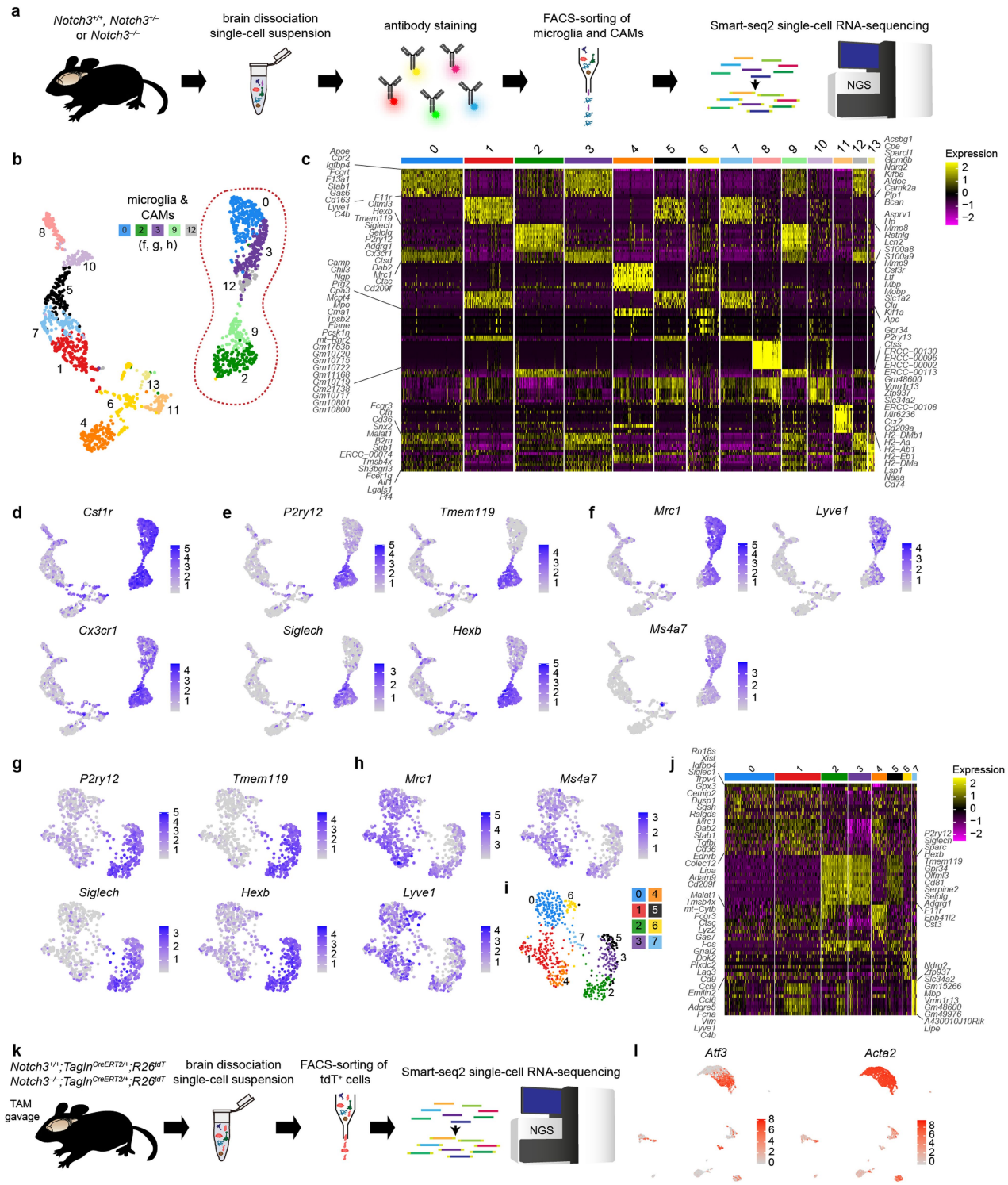

Extended Data Fig. 9 | Microglia and CAM transcriptomes are not affected by the loss of *Notch3*. (**a**) Scheme of the experimental set-up for the scRNA-seq analysis of brain macrophages from *Notch3* mice. (**b**) UMAP plot of 1523 individual cells isolated from P14 *Notch3*$^{+/+}$, *Notch3*$^{+/-}$ or *Notch3*$^{-/-}$ mice. Each dot represents an individual cell. Microglia and CAM clusters (0, 2, 3, 9 and 12) are framed with a dashed line. (**c**) Heat map of the top 10 differentially expressed genes for each cluster. (**d**) Feature plots depicting the expression of the typical brain macrophage genes *Csf1r* and *Cx3cr1*. (**e**, **f**) Feature plots showing the expression of microglial core genes (**d**) CAM core genes (**e**). (**g**–**j**) Re-analysis of the microglia and CAM clusters. Feature plots depicting the expression of microglial core genes (**g**) or CAM core genes (**h**). UMAP plot showing the individual clusters (**i**) and heat map (**j**) of the top 10 differentially expressed genes for each cluster. (**k**) Scheme of the experimental set-up for the scRNA-seq analysis of vascular smooth muscle cells from *Notch3*$^{+/+}$*SM22a*^{CreERT2}*R26*^{tdT} or *Notch3*$^{-/-}$*SM22a*^{CreERT2}*R26*^{tdT} mice. (**l**) Feature plots showing the expression of the arterial vascular smooth muscle cell core genes *Acta2* and *Aft3*.

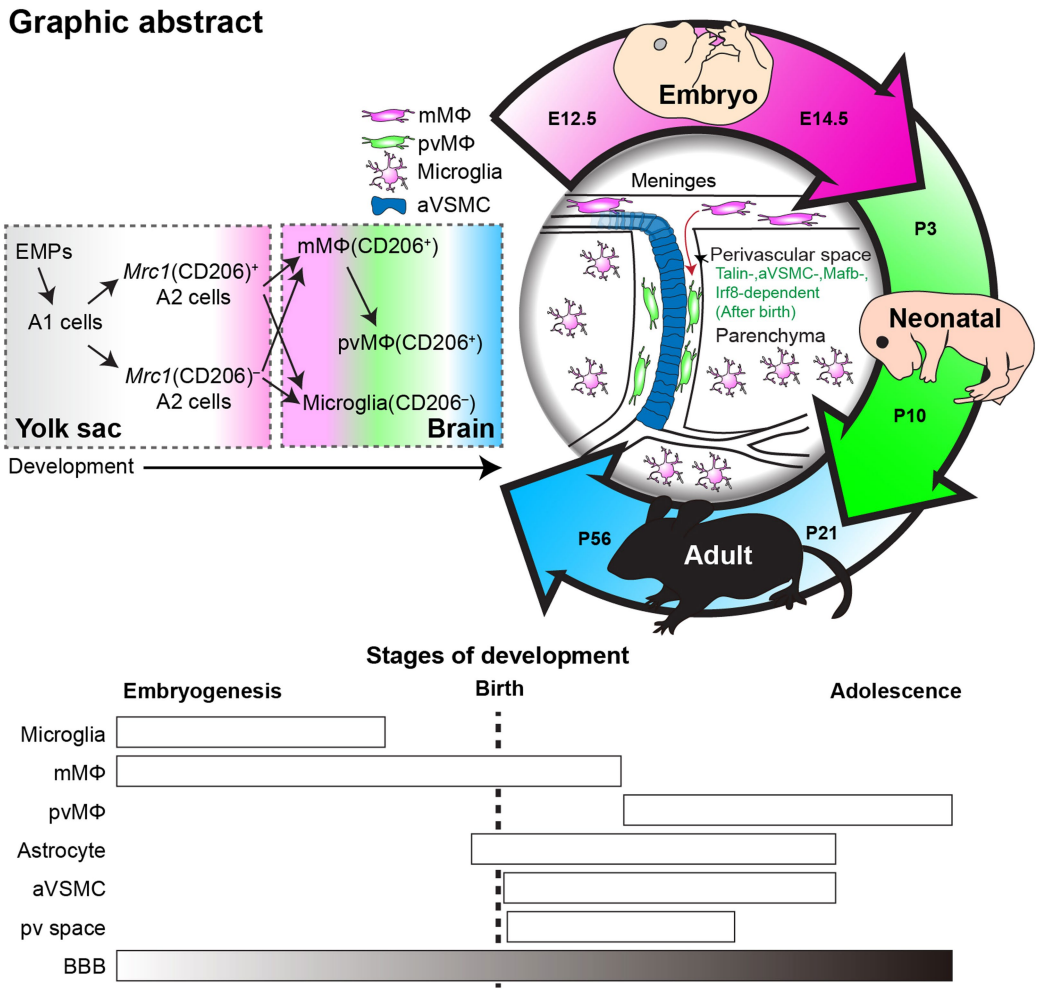

Extended Data Fig. 10 | Graphical abstract of experimental findings. Upper illustration depicts developmental trajectories of microglia and CAMs. Lower image shows stages of development in respective cell-types and blood brain barrier (BBB). EMPs: erythro-myeloid progenitors, mMΦ: meningeal macrophages, pvMΦ: perivascular macrophages, aVSMC: arterial vascular smooth muscle cells, pv: perivascular, E: embryonic days, P: postnatal days.

nature research

Corresponding author(s): Marco Prinz

Last updated by author(s): Feb 3, 2022

Reporting Summary

Nature Research wishes to improve the reproducibility of the work that we publish. This form provides structure for consistency and transparency in reporting. For further information on Nature Research policies, see our Editorial Policies and the Editorial Policy Checklist.

Statistics

For all statistical analyses, confirm that the following items are present in the figure legend, table legend, main text, or Methods section.

n/a	Confirmed	
☐	☒	The exact sample size (*n*) for each experimental group/condition, given as a discrete number and unit of measurement
☐	☒	A statement on whether measurements were taken from distinct samples or whether the same sample was measured repeatedly
☐	☒	The statistical test(s) used AND whether they are one- or two-sided *Only common tests should be described solely by name; describe more complex techniques in the Methods section.*
☒	☐	A description of all covariates tested
☐	☒	A description of any assumptions or corrections, such as tests of normality and adjustment for multiple comparisons
☐	☒	A full description of the statistical parameters including central tendency (e.g. means) or other basic estimates (e.g. regression coefficient) AND variation (e.g. standard deviation) or associated estimates of uncertainty (e.g. confidence intervals)
☐	☒	For null hypothesis testing, the test statistic (e.g. *F*, *t*, *r*) with confidence intervals, effect sizes, degrees of freedom and *P* value noted *Give P values as exact values whenever suitable.*
☒	☐	For Bayesian analysis, information on the choice of priors and Markov chain Monte Carlo settings
☒	☐	For hierarchical and complex designs, identification of the appropriate level for tests and full reporting of outcomes
☒	☐	Estimates of effect sizes (e.g. Cohen's *d*, Pearson's *r*), indicating how they were calculated

Our web collection on statistics for biologists contains articles on many of the points above.

Software and code

Policy information about availability of computer code

Data collection

RNA sequencing:
NextSeq 2000 Control Software (NCS) v1.2.0.36376 for the Illumina NextSeq 2000 instrument
HiSeq 1000 Control Software (HCS) v2.2.68 for the Illumina HiSeq 1000 instrument

bwa (version 0.6.2-r126) for transcriptome aligment of paired end reads (scRNA-seq)

Real Time Analysis Software (RTA) v3.7.17 and v2.4.11 software for image analysis and base calling and generation of .bcl files

bcl2fastq v2.20 software for conversion of .bcl files into fastq files

STAR aligner v2.7.8a (doi: 10.1093/bioinformatics/bts635) for sequence mapping/alignment to the mouse genome

featurecounts (version 1.5.1) for determination of gene count, available from
http://subread.sourceforge.net/

Microscopy:
FV10-ASW Ver.4.2a was used for confocal imaging with the Olympus FV 1000

Leica Application Suite (LAS) X 3.5.7.23225 was used for confocal imaging with the Leica TCS SP8 X

Data analysis

Seurat package for clustering of scRNA-seq data.
R package EnhancedVolcano to generate volcano plots.

R packages pheatmap and ggplot2 for generating heatmaps and barplots of bulk RNAseq data

GraphPad Prism 5.04 or 9 were used for statistical analysis.

For manuscripts utilizing custom algorithms or software that are central to the research but not yet described in published literature, software must be made available to editors and reviewers. We strongly encourage code deposition in a community repository (e.g. GitHub). See the Nature Research guidelines for submitting code & software for further information.

Data

Policy information about availability of data

All manuscripts must include a data availability statement. This statement should provide the following information, where applicable:

- Accession codes, unique identifiers, or web links for publicly available datasets
- A list of figures that have associated raw data
- A description of any restrictions on data availability

All data are available from the corresponding author on reasonable request.

Mouse reference genome: Gencode M26: https://www.gencodegenes.org/mouse/release_M26.html

All sequencing data has been uploaded to the Gene Expression Omnibus under the following accession codes:
Fig.4, Extended Data Fig.3: GSE194432 - Cell types dataset

Extended Data Fig.4 GSE194433 - CAM (Mrc1CreT2) dataset

Fig.2, Extended Data Fig5: GSE195437; the code is available at https://github.com/rsankowski/Taka_A1_A2_only

Figure 5, Extended Data Fig.9: GSE192585 - Notch3 microglia and macrophage data; GSE192510 - Notch3 brain dataset incl. vSMCs

Field-specific reporting

Please select the one below that is the best fit for your research. If you are not sure, read the appropriate sections before making your selection.

☒ Life sciences ☐ Behavioural & social sciences ☐ Ecological, evolutionary & environmental sciences

For a reference copy of the document with all sections, see nature.com/documents/nr-reporting-summary-flat.pdf

Life sciences study design

All studies must disclose on these points even when the disclosure is negative.

Sample size	No statistical methods were used to predetermine sample sizes. We ensured they were similar to those generally employed in the field for similar methods.
Data exclusions	Cells for scRNA-sequencing related to Fig.2 and Extended Data Fig.5, that failed during library preparation or had very low counts (less than 5000 reads mapped to mouse genes) were excluded. Also cells that were grouped as a cluster with less than 10 individual cells were excluded. Cells for scRNA-sequencing related to Fig.5h-j and Extended Data Fig.9b-j with high mitochondrial content, high spike-in content and low number of genes detected were discarded. Bulk RNA-seq related to Extended Data Figs.3+4: Genes with sum count expression less than 5 were filtered out. No other exclusions were made.
Replication	To be sure of the reproducibility of the experimental findings, we have usually used at least 3 individual mice from at least two independent experiments for each sample group. All replications were successful.
Randomization	Wherever applicable, mice used were randomly allocated into each experimental group. In most experiments, animals were grouped based on genotpye or age.
Blinding	During quantification of histological data, researchers were blind to the genotype of the animals whenever different genotypes were compared directy. In experiments were animals of the same genotype, but different ages were compared, blinding was not applied. This was due to the fact that imaging and quantification was done by the same researcher and differences in size and morphology of the CNS tissue prevented from complete blinding. Analysis of sequencing data, or protein expression/fluorescence intensities and percentage of reporter positive cells in flow cytometry was performed in an unbiased way based on software algorithms and/or positive/negative selection based on appropriate controls.

Reporting for specific materials, systems and methods

We require information from authors about some types of materials, experimental systems and methods used in many studies. Here, indicate whether each material, system or method listed is relevant to your study. If you are not sure if a list item applies to your research, read the appropriate section before selecting a response.

Materials & experimental systems

n/a	Involved in the study
☐	☒ Antibodies
☒	☐ Eukaryotic cell lines
☒	☐ Palaeontology and archaeology
☐	☒ Animals and other organisms
☐	☒ Human research participants
☒	☐ Clinical data
☒	☐ Dual use research of concern

Methods

n/a	Involved in the study
☒	☐ ChIP-seq
☐	☒ Flow cytometry
☒	☐ MRI-based neuroimaging

Antibodies

Antibodies used

Primary antibodies flow cytometry:
CD11b [M1/70] 1:300 (BV605, BioLegend, 101257, https://www.biolegend.com/en-us/products/brilliant-violet-605-anti-mouse-human-cd11b-antibody-7637?Clone=M1/70; BV421, BioLegend, 101251, https://www.biolegend.com/en-us/products/brilliant-violet-421-anti-mouse-human-cd11b-antibody-7163?Clone=M1/70)

CD45 [30-F11] 1:200 (APC-eF780, ThermoFisher Scientific, 47-0451-82, https://www.thermofisher.com/antibody/product/CD45-Antibody-clone-30-F11-Monoclonal/47-0451-82; FITC, BD Biosciences, 553079, https://www.bdbiosciences.com/en-us/products/reagents/flow-cytometry-reagents/research-reagents/single-color-antibodies-ruo/fitc-rat-anti-mouse-cd45.553079; APC, ThermoFisher Scientific, https://www.thermofisher.com/antibody/product/CD45-Antibody-clone-30-F11-Monoclonal/17-0451-82, PE-Cy7, ThermoFisher Scientific, 25-0451-82, https://www.thermofisher.com/antibody/product/CD45-Antibody-clone-30-F11-Monoclonal/25-0451-82)

Ly6C [AL-21] 1:200 (PerCP-Cy5.5, BD Biosciences, 560525, https://www.bdbiosciences.com/en-us/products/reagents/flow-cytometry-reagents/research-reagents/single-color-antibodies-ruo/percp-cy-5-5-rat-anti-mouse-ly-6c.560525; AF700, BD Biosciences, 561237, https://www.bdbiosciences.com/en-us/products/reagents/flow-cytometry-reagents/research-reagents/single-color-antibodies-ruo/alexa-fluor-700-rat-anti-mouse-ly-6c.561237)

Ly6G [1A8] 1:300 (APC-Cy7, BioLegend, 127623, https://www.biolegend.com/en-us/products/apc-cyanine7-anti-mouse-ly-6g-antibody-6755?Clone=1A8; BUV395, BD Biosciences, 565964, https://www.bdbiosciences.com/en-us/products/reagents/flow-cytometry-reagents/research-reagents/single-color-antibodies-ruo/buv395-rat-anti-mouse-ly-6g.565964)

Gr1 [RB6-8C5] 1:300 (PE, BioLegend, 108408, https://www.biolegend.com/en-us/products/pe-anti-mouse-ly-6g-ly-6c-gr-1-antibody-460?Clone=RB6-8C5)

CD115 [AFS98] 1:200 (PE-Cy7, ThermoFisher Scientific, 25-1152-82, https://www.thermofisher.com/antibody/product/CD115-c-fms-Antibody-clone-AFS98-Monoclonal/25-1152-82)

CD11c [N4A18] 1:300 (PE, ThermoFisher Scientific, 12-0114-81, https://www.thermofisher.com/antibody/product/CD11c-Antibody-clone-N418-Monoclonal/12-0114-81)

F4/80 [BM8] 1:200 (PE-Cy7, ThermoFisher Scientific, 25-4801-82, https://www.thermofisher.com/antibody/product/F4-80-Antibody-clone-BM8-Monoclonal/25-4801-82)

CD3e [eBio500A2[1:300 (eFluor 450, ThermoFisher Scientific, 48-0033-82, https://www.thermofisher.com/antibody/product/CD3e-Antibody-clone-eBio500A2-500A2-Monoclonal/48-0033-82)

CD19 [eBio1D3] 1:200 (eFluor 450, ThermoFisher Scientific, 48-0193-82, https://www.thermofisher.com/antibody/product/CD19-Antibody-clone-eBio1D3-1D3-Monoclonal/48-0193-82)

CD206 [C068C2] 1:200 (APC, BioLegend, 141708, https://www.biolegend.com/en-us/products/apc-anti-mouse-cd206-mmr-antibody-7425?Clone=C068C2; FITC, BioLegend, 141704, https://www.biolegend.com/en-us/products/fitc-anti-mouse-cd206-mmr-antibody-7318?Clone=C068C2)

CD93 [AA4.1], 1:200 (PerCP-Cy5.5, BioLegend, 136511, https://www.biolegend.com/en-us/products/percp-cyanine5-5-anti-mouse-cd93-aa4-1-early-b-lineage-antibody-6862?Clone=AA4.1)

c-Kit/CD117 [2B8] 1:200 (PE-Cy7, BioLegend, 105814, https://www.biolegend.com/en-us/products/pe-cyanine7-anti-mouse-cd117-c-kit-antibody-1900?Clone=2B8; APC-Cy7, BioLegend, 105826, https://www.biolegend.com/en-us/products/apc-cyanine7-anti-mouse-cd117-c-kit-antibody-5905?Clone=2B8; BV605, BioLegend, 105847, https://www.biolegend.com/en-us/products/brilliant-violet-605-anti-mouse-cd117-c-kit-antibody-16969?Clone=2B8)

Sca1 [D7] 1:200 (BUV395, BD Biosciences, 563990, https://www.bdbiosciences.com/en-us/products/reagents/flow-cytometry-reagents/research-reagents/single-color-antibodies-ruo/buv395-rat-anti-mouse-ly-6a-e.563990)

CD48 [HM48-1] 1:200 (APC, BioLegend, 103412, https://www.biolegend.com/en-us/products/apc-anti-mouse-cd48-antibody-3622?Clone=HM48-1)

CD150 [TC15-12F12.2] 1:200 (PE-Cy7, BioLegend, 115914, https://www.biolegend.com/en-us/products/pe-cyanine7-anti-mouse-

cd150-slam-antibody-3056?Clone=TC15-12F12.2)

Primary ABs for histological analysis in mice:
Iba1 [EPR16588] 1:1000 (Abcam, ab178846, https://www.abcam.com/iba1-antibody-epr16588-ab178846.html)

Iba1 [polyclonal] 1:1000 (Synaptic Systems, 234004, https://sysy.com/product/234004)

CD206 [MR5D3] 1:500 (Bio-Rad, MCA2235, https://www.bio-rad-antibodies.com/monoclonal/mouse-cd206-antibody-mr5d3-mca2235.html?f=purified)

CD206 [polyclonal] 1:500 (R&D Systems, AF2535, https://www.rndsystems.com/products/mouse-mmr-cd206-antibody_af2535)

collagen IV [polyclonal] 1:200 (Millipore, AB769, https://www.merckmillipore.com/DE/de/product/Anti-Collagen-Type-IV-Antibody,MM_NF-AB769)

laminin [polyclonal] 1:1000 (ThermoFisher Scientific, PA1-16730, https://www.thermofisher.com/antibody/product/Laminin-Antibody-Polyclonal/PA1-16730)

transferrin receptor [8D3] 1:500 (Novus Biologicals, NB100-64979, https://www.novusbio.com/products/tfr-transferrin-r-antibody-8d3_nb100-64979)

alpha smooth muscle actin [1A4] 1:200 (ThermoFisher Scientific, 14-9760-82, https://www.thermofisher.com/antibody/product/Alpha-Smooth-Muscle-Actin-Antibody-clone-1A4-Monoclonal/14-9760-82)

NeuN [Clone60] 1:500 (Millipore, MAB377, https://www.merckmillipore.com/DE/de/product/Anti-NeuN-Antibody-clone-A60,MM_NF-MAB377)

APC [CC-1] 1:500 (Millipore, OB80, https://www.merckmillipore.com/DE/de/product/Anti-APC-Ab-7-Mouse-mAb-CC-1,EMD_BIO-OP80)

GFP [polyclonal] (Abcam, ab13970, https://www.abcam.com/gfp-antibody-ab13970.html?productWallTab=ShowAll)

SOX9 [polyclonal] 1:500 (R&D Systems, AF3075, https://www.rndsystems.com/products/human-sox9-antibody_af3075)

P2Y12R [polyclonal] 1:500 (Anaspec, AS-55043A, Note: product has been discontinued)

Lyve1 [ALY7] 1:500 (ThermoFisher Scientific, 14-0443-82, https://www.thermofisher.com/antibody/product/LYVE1-Antibody-clone-ALY7-Monoclonal/14-0443-82)

Ki-67 [polyclonal] 1:500 (Abcam, ab15580, https://www.abcam.com/ki67-antibody-ab15580.html)

Ki-67 rat [SolA15] 1:500 [ThermoFisher Scientific, 14-5698-82, https://www.thermofisher.com/antibody/product/Ki-67-Antibody-clone-SolA15-Monoclonal/14-5698-82)

active Caspase3 [C92-605] 1:500 (BD Biosciences, 559565, https://www.bdbiosciences.com/en-nz/products/reagents/flow-cytometry-reagents/research-reagents/single-color-antibodies-ruo/purified-rabbit-anti-active-caspase-3.559565)

F4/80 [BM8] 1:500 (BioLegend, 123101, https://www.biolegend.com/en-us/products/purified-anti-mouse-f4-80-antibody-4064?Clone=BM8)

Fibrinogen [polyclonal] 1:1000 (US Biological, F4203-02F, https://www.usbio.net/antibodies/F4203-02)

Claudin 5 [4C3C2] 1:200 (Invitrogen, 352588, https://www.thermofisher.com/antibody/product/Claudin-5-Antibody-clone-4C3C2-Monoclonal/352588)

Secondary ABs for immunofluorescence in mice were ordered from ThermoFisher Scientific or Jackson Laboratory and added as follows:
Alexa Flour® 405 1:1000,

Alexa Flour® 488 1:1000,

Alexa Flour® 568 1:1000

Alexa Fluor® 647 1:1000

For histological analysis in human:
CD206 [5C11] 1:300 (Abnova, H00004360-M02, http://www.abnova.com/products/products_detail.asp?catalog_id=H00004360-M02)

Collagen IV [IHC549] 1:1000 (GenomeMe, IHC549-100, https://www.genomeme.ca/ihc-antibodies/Collagen-Type-IV-IHC549/)

P2ry12 [polyclonal] 1:500 (Sigma, HPA014518, https://www.sigmaaldrich.com/DE/en/product/sigma/hpa014518)

Validation

All primary antibodies used for flow cytometry, immunofluorescence, immunohistochemistry have been validated for this application in the respective species (mouse or human) by the supplier and have been used in previous studies. For validation methods and

references please follow the provided links to the product websites.

Fluorescence minus one stains or isotype controls were used to define cell popualation-gates for FACS sorting and to define gates for positive/negative selection for all flow cytometry-based quantifications.

Further, positive controls were included for every experiment to ensure that the ABs worked in prinicple.

Animals and other organisms

Policy information about studies involving animals; ARRIVE guidelines recommended for reporting animal research

Laboratory animals	Mice of both gender were used for the experiments. Mice of an age starting from embryonic day (E)8.5 to adult mice (8weeks) were used for the experiments. The age of experimental animal used is depicted in the experimental schemes and/or figure legends for every experiments. C57BL/6N mice were used as wild-type mice. Transgenic lines including Cx3cr1GFP (B6.129P2(Cg)-Cx3cr1tm1Litt/J), Cx3cr1Cre (B6J.B6N(Cg)-Cx3cr1tm1.1(cre)Jung/J), Cx3cr1CreERT2 (B6.129P2(C)-Cx3cr1tm2.1(cre/ERT2)Jung/J), HexbCreERT2(ref18), Cxcr4CreERT2-Ires-YFP (Cxcr4CreERT2)29, SMMHCCreERT2 (B6.FVB-Tg(Myh11-cre/ERT2)1Soff/J), VavCre (ref48), Tln1fl(ref49), Fgf2-/- (ref50), Pdgfrb-/F7 (ref40), Notch3-/- (ref43,51), Rbpjfl (ref44), Itgb1fl (ref52), Irf8fl (ref53), R26tdT (Jackson Lab, #007914), R26YFP (Jackson Lab, #006148), R26Confetti (ref54), Lyve1CreERT2 (B6/JGpt- Lyve1-CreERT2, GemPharmatech Co., Ltd, Nanjing, China) and Taglntm1(cre/ERT2)Feil mice were used in this study. Rbpjfl mice were kindly provided by Riken, Japan (RBRC01071). Mafbfl mice55 were kindly provided by Dr. Goodrich, President and Fellows of Harvard College. Mice were bred in-house under pathogen-free conditions with a 12 hour light/dark cycle.
Wild animals	No wild animals were used in this study.
Field-collected samples	No field collected samples were used in this study.
Ethics oversight	An ethics statement is provided in the methods section. The Regierungspräsidium Freiburg, Germany, or the Institutional Animal Care and Use committee review panels at Kyushu University, Japan, have approved all animal experiments.

Note that full information on the approval of the study protocol must also be provided in the manuscript.

Human research participants

Policy information about studies involving human research participants

Population characteristics	In the present study, human fetal brain specimens from artificial abortions and brains from dead newborns are used. The age ranges from the 20th gestational week to 4 weeks of age. Both sexes, male and female, were included. A trained neuropathologist ensured that none of the specimens showed neuropathological abnormalities and that the brain tissue macroscopically and microscopically was according to the respective age. Furthermore, no genetic defects were known.
Recruitment	The specimens derive from patients that underwent autopsy after death. The responsible clinicians requested the autopsy to clarify the cause of the death. The patients or their respective legal guardians gave their informed consent.
Ethics oversight	The University of Freiburg Medical Center gave ethics approval (approval number 10008/09). All experiments with embryonal and newborn brain tissue were performed in accordance with the Declaration of Helsinki and the local regulations.

Note that full information on the approval of the study protocol must also be provided in the manuscript.

Flow Cytometry

Plots

Confirm that:

☒ The axis labels state the marker and fluorochrome used (e.g. CD4-FITC).

☒ The axis scales are clearly visible. Include numbers along axes only for bottom left plot of group (a 'group' is an analysis of identical markers).

☒ All plots are contour plots with outliers or pseudocolor plots.

☒ A numerical value for number of cells or percentage (with statistics) is provided.

Methodology

Sample preparation	After taking out from pregnant females, extraembryonic YS was homogenized with syringes in HBSS containing 15 mM HEPES buffer and 0.54 % glucose. After spinning down, the pellet containing the YS progenitors at the bottom of the tube was then collected and washed once with FACS Buffer (PBS containing 2 % FCS and 10mM EDTA) before staining. The single cell suspension was used for the staining procedure as described14. FC receptors were blocked with Fc Block (2.4G2, BD Biosciences) for 10 min at 4 °C prior to incubation with the primary antibodies. Cells were stained with fluorophore-conjugated for 45 min at 4 °C in FACS buffer.
Instrument	Cells were sorted using a MoFlo Astrios (Beckman Coulter) or analyzed using a BD LSRFortessa (Becton Dickinson)

Software	Data were acquired with FACSDiva software (Becton Dickinson). Postacquisition analysis was performed using FlowJo software, version 10.5.3.
Cell population abundance	The cell population abundances are provided in the plots depicting the representative gating strategies of each experiment.
Gating strategy	In all experiments, small debris was removed with the preliminary FSC/SSC gate. Single, living cells were obtained by doublet exclusion and exlusion of dead cells with live-dead dyes or DAPI. Further, gating strategies for the respective experiments are provided in the figurse.

☒ Tick this box to confirm that a figure exemplifying the gating strategy is provided in the Supplementary Information.